AD_____

Award Number: W81XWH-11-1-0357

TITLE: New Treatments for Drug-Resistant Epilepsy that Target Presynaptic Transmitter Release

PRINCIPAL INVESTIGATOR: Dr. Patric Stanton

CONTRACTING ORGANIZATION: New York Medical College
Valhalla, NY 10595

REPORT DATE: May 2012

TYPE OF REPORT: Annual

PREPARED FOR: U.S. Army Medical Research and Materiel Command
Fort Detrick, Maryland 21702-5012

DISTRIBUTION STATEMENT: Approved for public release; distribution unlimited

REPORT DOCUMENTATION PAGE

Form Approved
OMB No. 0704-0188

1. REPORT DATE *(DD-MM-YYYY)*	2. REPORT TYPE	3. DATES COVERED *(From - To)*
01-05-2012	Annual	15 Apr 2011 - 14 Apr 2012

4. TITLE AND SUBTITLE
New Treatments for Drug-Resistant Epilepsy that Target Presynaptic Transmitter Release

5a. CONTRACT NUMBER

5b. GRANT NUMBER
W81XWH-11-1-0357

5c. PROGRAM ELEMENT NUMBER

6. AUTHOR(S)
Dr. Patric Stanton

E-Mail: patric_stanton@nymc.edu

5d. PROJECT NUMBER

5e. TASK NUMBER

5f. WORK UNIT NUMBER

7. PERFORMING ORGANIZATION NAME(S) AND ADDRESS(ES)
New York Medical College
Valhalla, NY 10595

8. PERFORMING ORGANIZATION REPORT NUMBER

9. SPONSORING / MONITORING AGENCY NAME(S) AND ADDRESS(ES)
U.S. Army Medical Research and Materiel Command
Fort Detrick, Maryland 21702-5012

10. SPONSOR/MONITOR'S ACRONYM(S)

11. SPONSOR/MONITOR'S REPORT NUMBER(S)

12. DISTRIBUTION / AVAILABILITY STATEMENT
Approved for Public Release; Distribution Unlimited

13. SUPPLEMENTARY NOTES

14. ABSTRACT

In year 01, we completed the majority of our studies in Aim 1 and a portion of Aim 2. We found, in both rats and mice, that severe pilocarpine-induced seizures that result in long-term appearance of spontaneous epileptic seizures are associated with marked changes in the structure of hippocampal mossy fiber presynaptic terminals and functional hyperexcitability of presynaptic vesicular transmitter release. Mossy fiber terminals as a whole, their transmitter release active zone and readilyreleasable vesicle pool, were greatly increased in size, and there was even sprouting of new mossy fiber terminals into regions where they do not normally synapse. Functionally, these presynaptic glutamatergic terminals showed greatly enhanced rate of vesicular release from the rapidly-recycling vesicle pool and accelerated endocytotic recycling of vesicles. We commenced studies to be completed in year 02 to test the ability of four antiepileptic drugs that act via differing mechanisms (levetiracetam, lamotrigine, carbamezipine and topiramate), to control presynaptic vesicular release two months after pilocarpine-induced seizures, when the brain has become spontaneously epileptic. We also discovered that the presynaptic vesicle protein dynamin, which is an essential component of one vesicle recycling pathway, is markedly down-regulated in expression and the dynamin pathway loses its ability to keep up with vesicular release in the epileptic brain. If we can find agents that can control presynaptic release, and do so even after development of epilepsy when release is enhanced, we would have a whole new class of treatments to help the 40% of epileptic patients who do not respond to any current therapeutics.

15. SUBJECT TERMS
No subject terms provided.

16. SECURITY CLASSIFICATION OF:			17. LIMITATION OF ABSTRACT	18. NUMBER OF PAGES	19a. NAME OF RESPONSIBLE PERSON
a. REPORT	b. ABSTRACT	c. THIS PAGE			USAMRMC
U	U	U	UU	38	19b. TELEPHONE NUMBER *(include area code)*

Table of Contents

PROGRESS REPORT: DoD Grant - PR100534P1

Title: *New Treatments for Drug-Resistant Epilepsy that Target Presynaptic Transmitter Release*

Principal Investigator: Patric K. Stanton, PhD
Department of Cell Biology & Anatomy, New York Medical College (NYMC), Valhalla, NY

INTRODUCTION

Posttraumatic epilepsy is a major long-term complication of traumatic brain injury (TBI), that usually develops within 5 years of head injury (Schauwecker, 2012), and is often expressed as medically intractable hippocampal epilepsy (Turski et al., 1984; Muller et al., 2009). Posttraumatic epilepsy can develop after penetrating or severe non-penetrating brain injury. Although there are a variety of causes of traumatic epilepsy, the resulting chronic neurological condition is characterized by common features, including recurrent spontaneous seizures, neuronal damage, and, in ~30% of mesial temporal lobe epileptic (MTLE) patients, resistance to all available anticonvulsant drugs (Li et al., 2005; Burrone et al., 2006). ***Therefore, it is of critical importance to develop novel models to study post-traumatic epilepsy, to facilitate discovery of new treatments.*** During epileptogenesis, seizure-related functional and structural reorganization of neuronal circuits leads to both hyperexcitability of glutamatergic neurons and defective inhibition (Mello et al., 1993; Upreti et al., 2012). While many postsynaptic alterations have been demonstrated, there is surprisingly little known concerning dysfunction of presynaptic transmitter release machinery in epilepsy. The recent successful introduction of the antiepileptic drug levetiracetam (LEV; Boulland et al., 2007), which acts on presynaptic molecular targets, suggests that controlling dysregulation of presynaptic function could be a promising new therapeutic target for the treatment of unresponsive epilepsies. While LEV has been shown to bind to both the synaptic vesicle protein SV2a and N-type Ca^{2+} channels (Epsztein et al., 2005; Esclapez et al., 1999; Pacheco Otalora et al., 2006), its precise mechanism of action is not understood.

BODY

HYPOTHESIS AND OBJECTIVES:

During periods of intense neuronal activity such as seizures, a larger pool of vesicles could result in more glutamate being released and long-lasting aberrant excitation. We propose to explore the effects of seizures on transmitter release and the presynaptic action of AEDs on these changes. We will use electrophysiology and multiphoton confocal microscopy. Preliminary data indicate that SE induces long-lasting potentiation of synaptic vesicle release in epileptic rats. We hypothesize that successful AED treatment might prevent or reverse these seizure-induced molecular deficiencies (reduction of N-type VGCC, mGluR II and SV2a expression), and be antiepileptogenic as well. Our **central hypothesis** is that pharmacological regulation of glutamate transmitter release at presynaptic sites will be an effective, novel therapeutic strategy to ameliorate epileptogenesis and excessive synaptic excitation in epilepsy. The **long-term objectives** of this collaborative proposal are to: (1) identify the most effective AEDs which modulate presynaptic glutamate release, and (2) determine the presynaptic mechanism of action of the new AED LEV to modulate vesicular release properties. *Our central hypothesis is that pharmacological regulation of glutamate transmitter release at presynaptic sites will be an effective, novel therapeutic strategy to treat many cases of drug-resistant epilepsy, especially epileptogenesis following traumatic brain injury.* The **long-term goals** of this collaborative project are to: (1) identify the most effective antiepileptic drugs amongst compounds that modulate presynaptic glutamate release and (2) determine the presynaptic mechanism of action of the new antiepileptic drug **levetiracetam** (LEV). ***In Year 1 of this proposal, we completed experiments that accomplished the vast majority of specific Aim 1 Task 1, our portion of year 01 of the collaborative project, as outlined below.***

Specific Aim 1: *Determine which antiepileptic drugs are most effective at reducing glutamate release from mossy fiber presynaptic boutons (MFBs) in the pilocarpine model of mesial temporal lobe epilepsy (MTLE)* (months 1-12).

Working hypothesis: Drugs acting on presynaptic Ca^{2+} channels, autoreceptors, and SV2a will be more effective in reducing vesicular glutamate release at excitatory presynaptic terminals in the hippocampus.

Research Accomplishments:

Task 1. Evaluate the effects of different concentrations of "classical" (*e.g*. carbamazepine, lamotrigine, and topiramate, and "new generation" antiepileptic drugs (*e.g.* LEV) on presynaptic glutamate release by using two-photon imaging of vesicular release of the fluorescent dye FM1-43 from individual mossy fiber terminals in *in vitro* hippocampal slices.

Development of the pilocarpine model of epilepsy in mice and rats at both institutions. (Subtask 1a) single injection of pilocarpine in rats and in the transgenic Sp21 mice expressing the fluorescent reporter of synaptic vesicle release and presynaptic function synaptophlourin (SpH).

YEAR 01 Stanton Lab

- **Subtask 1a.** Develop chronic epileptic rats with a single injection of pilocarpine (Dr. Garrido, Dr. Pacheco, Dr. Stanton and Dr. Upreti; months 1-12).
- **Subtask 1b.** Prepare hippocampal slices from control and epileptic rats (Dr. Stanton, Dr. Upreti; months 1-12).
- **Subtask 1c.** Image presynaptic transmitter release from individual mossy fiber terminals using two-photon confocal laser scanning microscopy of the fluorescent dye FM1-43 (Dr. Stanton, Dr. Zhang and Dr. Upreti; months 1-12).
- **Subtask 1d.** Test whether antiepileptic drugs modify kinetics of transmitter release in control versus epileptic rats (Dr. Stanton, Dr. Zhang and Dr. Upreti; months 1-12).
- **Subtask 1c.** Statistical analysis of the experimental data (Dr. Stanton, Dr. Zhang and Dr. Upreti, months 9-12).

1.a and 1.b. Developed the pilocarpine model of epilepsy in mice and rats at NYMC and UTB:

Colonies of chronically epileptic Sprague Dawley rats and SynaptopHlourin (SpH) mice were established at both New York Medical College (NYMC) and the University of Texas at Brownsville (UTB), using protocols validated in Dr. Garrido's laboratory (**Subtask 1a)**. In addition, the pilocarpine model of mesial temporal lobe epilepsy (MTLE) was also developed in the SV2A/SV2B knockout mice at the laboratory of Dr. Garrido. Hippocampal slices for multiphoton laser scanning confocal imaging analysis of presynaptic release (Dr. Stanton, NYMC) and *in vitro* electrophysiology (Dr. Garrido, UTB) were obtained from control and epileptic rats and transgenic mice (**Subtask 1b**).

Development of the pilocarpine model in SpH and SV2A knockout mice: Previous studies have reported differential susceptibility of mouse strain to pilocarpine-induced *status epilepticus* and seizure-induced excitotoxic cell death (Schauwecker, 2012). Therefore, in close collaboration with the laboratory of Dr. Garrido-Sanabria at UTB, we optimized and fully characterized the pilocarpine model in SpH-expressing mice (Sp21 variant), which express a fusion protein of vesicle-associated membrane protein 2 (*Vamp2*) and a pH-sensitive green fluorescence protein under the control of the mouse thymus cell antigen 1 (*Thy1*) promoter, which drives expression of SpH in granule cells of dentate gyrus and their mossy fiber axons and presynaptic boutons in *stratum lucidum* of the hippocampus. Breeders were obtained from Jackson Laboratories *i.e.* B6.CBA-Tg(Thy1-spH)21Vnmu/J, C57BL/6J (Stock Number: 014651) to establish the colony Dr. Garrido's laboratory, while this same strain was already available at Dr. Stanton's Laboratory (kind gift of Dr. Venkatesh Murthy, Harvard University). For the induction of *status epilepticus* animals received methylscopolamine nitrate (0.1 mg/kg in saline, s.c.) thirty minutes before pilocarpine to minimize peripheral effects of cholinergic stimulation (Turski et al.,

1984). Thereafter, pilocarpine hydrochloride (350mg/kg) was intraperitoneally injected using different doses (300, 320, 350 and 380 mg/kg of body weight, 5 animals per group). The dose used was most efficient, yielding 90% of animals entering *status epilepticus* and 80% survival rate. After animals entered *status epilepticus*, a second dose of methylscopolamine was subcutaneously injected and animals were allowed to seize for 1 hour, after which motor seizures were terminated with injection of diazepam (10 mg/kg in saline *i.p*.). Only animals experiencing continuous SE during these periods were studied. Control animals received methylscopolamine and saline instead of pilocarpine. This pilocarpine model of mesial temporal lobe epilepsy was also optimized in wild type, heterozygous and knockout SV2A mice obtained from Jackson Laboratories (Stock number: 006383, B6; 129P2-*Sv2a*^{tm1Sud} *Sv2b*^{tm1Sud}/J). These animals were developed with the same genetic background (C57BL/6J) of the SpH21 mice. Accordingly, the same concentrations of methylscopolamine and pilocarpine were used following the same protocol as for SpH mice. *Now that we have extended the pilocarpine model to SV2A knockout mice, these animals will be employed in the Stanton laboratory to evaluate the role of SV2A and targeting of this protein by levetiracetam in seizure-induced enhancement of mossy fiber presynaptic vesicular release, and in the Garrido-Sanabria laboratory to examine its importance to excitatory activation of dentate granule cells using whole-cell recordings (Task 2).*

1.c.1 Two-photon laser scanning microscopy imaging of vesicular transmitter release from large mossy fiber boutons of epileptic rats and synaptopHluorin (SpH)-expressing mice.

Two-photon laser scanning microscopy imaging of large mossy fiber boutons of synaptopHluorin expressing transgenic mice in acute hippocampal slices – a new model to directly image presynaptic transmitter release during epilepsy

SynaptopHluorin (SpH) is a fusion protein that consists of a pH sensitive eGFP (pHluorin) fused to the C-terminus luminal domain of the vesicle SNARE protein synaptobrevin (Miesenbock *et al.*, 1998). Under resting conditions, the luminal pH of the synaptic vesicle is acidic (pH~5.5), resulting in proton dependent quenching of SpH fluorescence. When vesicle exocytosis is triggered and glutamate released, the lumen of the vesicle is exposed to the more alkaline pH of the extracellular space (pH~7.2), resulting in a 20-fold increase in SpH fluorescence. When the vesicle membrane is retrieved by endocytosis and the vesicle reformed, it undergoes rapid reacidification by the vesicular ATPase, which returns SpH to its quenched state. The SpH21 transgenic mice line we used in this study, expresses SpH preferentially at glutamatergic synapses (Li *et al.*, 2005; Burrone *et al.*, 2006; Bayazitov *et al.*, 2007). Representative two photon laser scanning image of the CA3 region of an acute hippocampal slice from this mouse (Figure. 1A) contains bright GFP positive boutons >2 μm in diameter, proximal to CA3 pyramidal cell bodies in the region innervated by mossy fiber axons of dentate granule cells (Blackstad *et al.*, 1970; Claiborne *et al.*, 1986). Associational-commissural CA3 synapses are significantly smaller (<1 μm in diameter) and more distal to our region of interest (rectangular box, Figure 1A).

To confirm that large SpH expressing boutons were mossy fiber terminals, we used anterograde, bulk labeling of mossy fibers with Alexa Fluor 594 dextran introduced into the granule cell layer of the dentate gyrus (Figure 1B). During a 1.5-2 hour incubation, Alexa Fluor 594 dextran was taken up by granule cells and transported anterogradely to label mossy fiber axons and presynaptic boutons (Figure 1C). Figures 1E and 1F illustrate that some (solid arrows) but not all (broken arrows) SpH and Alexa Fluor 594-positive boutons were co-labeled confirming that, indeed, the large (>2μm in diameter) SpH fluorescent puncta within the proximal 60 μm of the CA3 cell body are the excitatory mossy fiber boutons (Figure. 1D). Associational-commissural CA3 synapses are significantly smaller (<1μm in diameter) and more distal to our region of interest (rectangular box, Fig. 1A). Incomplete co-localization is likely because Alexa Fluor 594-labeled a subset of mossy fiber axons in *stratum lucidum* in addition to sparse SpH expression in the excitatory terminals (Li *et al.*, 2005; Burrone *et al.*, 2006).

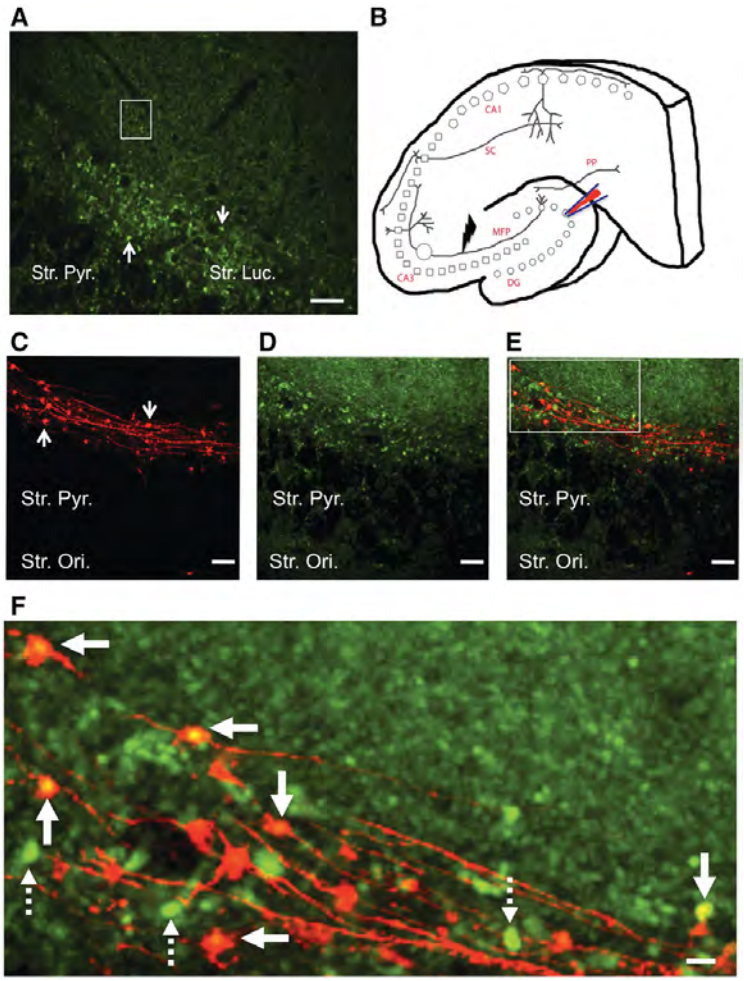

Figure 1: Visualizing mossy fiber boutons (MFBs) in acute hippocampal slices from SpH21 transgenic mice line. **(A)** Live cell two photon laser scanning image of field CA3 of SpH expressing glutamatergic terminals in a control hippocampal slice (postnatal 60 days). The arrows depict representative fluorescence puncta (about 4-5 µm in diameter) in the proximal (*stratum lucidum*) region of CA3 pyramidal cells (seen here as a ghost layer) that are likely to be giant MFBs. Distal puncta shown within the rectangular box are notably smaller in size and likely represent the associational-commissural synapses in the *stratum radiatum*. *Stratum pyramidale* (Str. Pyr.) and *Stratum Oriens* (Str. Ori.). Scale bar = 20 µm. **(B)** Cartoon representing the hippocampal circuitry with the circle in the mossy fiber pathway (MFP) depicting the area of imaging, depicts the area of local stimulation and the pipette in the dentate granule cell layer (DG) shows the area of Alexa Fluor 594 dextra containing pipette insertion. (PP: perforant path, SC: Schaffer collaterals, squares and pentagons depict CA3 and CA1 pyramidal cell layers respectively). **(C)** Alexa Fluor 594 dextran filled MF axons and giant MFB (arrows) showing characteristic en-passant arrangement along the axonal projections, visualized using 825nm excitation. **(D)** Same region as (**C**) but visualized with 890nm excitation to see SpH native fluorescence. CA3 pyramidal cell bodies can be seen as ghost cells in stratum pyramidal (Str. Pyr), and bright giant MFB in *stratum lucidum*. Scale bar = 20 µm (**C-E**). **(E-F)** Merged images of (**C**) and (**D**) show colocalization (f: arrows) between SpH and Alexa Fluor 594 dextran-labeled puncta. (**F**) Digital zoom of image from inset box in (**E**), scale bar = 4 µm. Not all SpH-positive puncta colocalized with Alexa Fluor 594 (F: broken arrows).

Pilocarpine-induced status epilepticus persistently increases size, vesicular release rate and endocytosis of mossy fiber boutons in SpH-expressing mice

Size: Live cell imaging of mossy fiber boutons in acute hippocampal slices was done by bulk loading a group of granule cells and their axons with Alexa Fluor 594-dextran. Dye-filled excrescences (Figure. 2A) were classified as the main body of giant mossy fiber boutons if they had at least a 4µm^2 cross-sectional area (Claiborne *et al.*, 1986; Acsady *et al.*, 1998; Danzer *et al.*, 2010). The mean area of mossy fiber boutons 1-2 months after pilocarpine induced-SE were significantly enhanced (~21.09%, Fig. 4C, *P*=0.008, Mann-Whitney U-test, *n*=7) when compared to aged matched controls (*n*=7). A frequency distribution histogram of individual mossy fiber boutons from epileptic animals revealed a significant rightward shift in the curves (Fig. 2B; *P* <0.05 Kolgomorov-Smirnov test) and an overall significant increase in mossy fiber bouton imaging area (Fig. 2C; *P*<0.05, Mann-Whitney U-test).

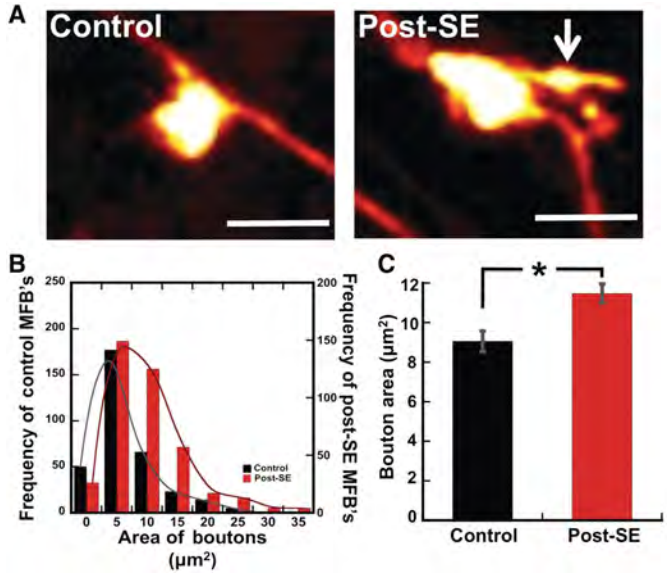

Figure 2: Pilocarpine-induced SE leads to persistent increase in dentate gyrus giant MFB area. (A) Live cell two-photon images of Alexa Fluor 594 dextran loaded giant mossy fiber terminals from field CA3 of acute hippocampal slices from control and post-SE mice. The arrow shows a filopodia-like projection arising from the giant MFB. Scale bar = 5 μ m. **(B)** Frequency distribution histogram of individual MFBs area from control (black columns, total of 336 boutons, *n*=7) and 1-2 months post-SE mice (red columns, 394 boutons, *n*=7). (**C**) Mean MFB area for control (black column, 9.05 ± 0.52 μm^2) and epileptic (red column, 11.47 ± 0.48 μm^2) mice. Data plotted as mean ± SEM, * *P*<0.05, Mann-Whitney U-test.

Vesicular Exocytosis: To determine whether post-SE leads to functional differences in transmitter release from excitatory mossy fiber boutons we utilized two-photon live cell imaging in slices from SpH21 mice. To trigger vesicular release from mossy fiber boutons in CA3 *stratum lucidum* (Fig. 1B-F), slices from control and post-SE animals were stimulated with a single, continuous train of 600 stimuli at 20Hz (Fig. 2B), a paradigm that recruits both the RRP and rapidly recycling vesicle pools (Li *et al.*, 2005). Representative time lapse images (Figure 3A) of control and post-SE SpH expressing mossy fiber boutons (solid arrows) showed robust, cumulative increases in SpH fluorescence intensity during the stimulus train, followed by return of fluorescence to baseline levels ~40 sec after stimulus termination (Figure 3B). Figure 3C plots the normalized mean SpH fluorescence responses in control versus post-SE animals, which showed significantly larger stimulus-evoked increases in SpH fluorescence (2.02 ± 0.15, red circles, *n*=8, *P*<0.05, Student's t-test) compared to controls (1.47 ± 0.03, black circles, *n*=10).

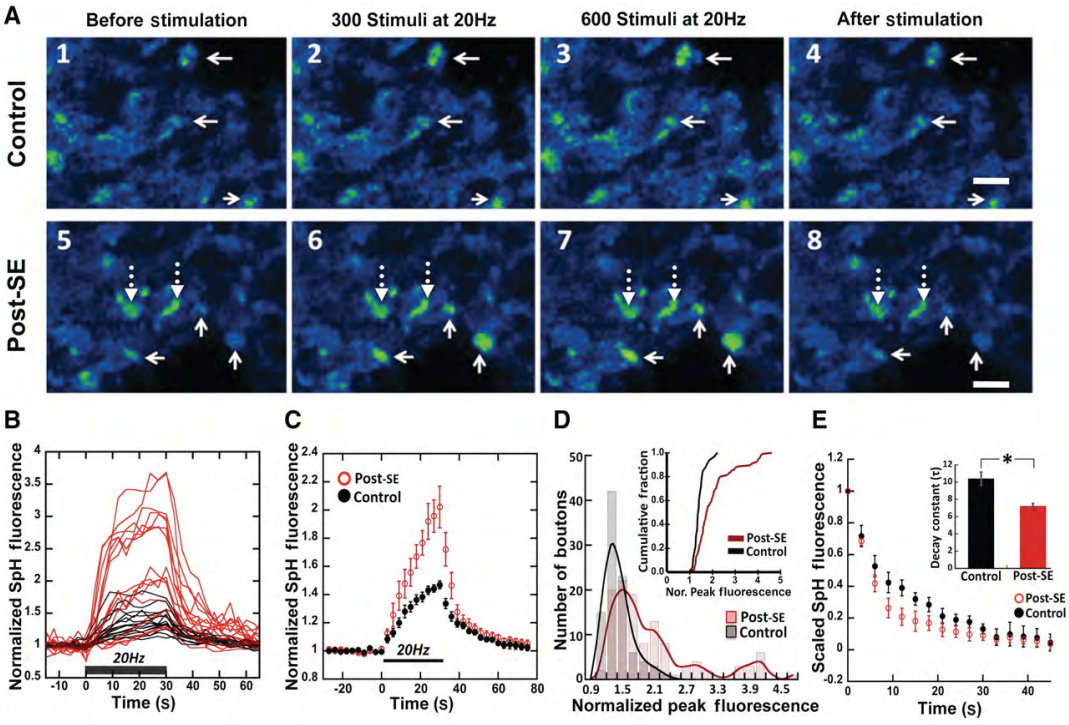

Figure 3: Pilocarpine-induced SE enhances vesicular release and endocytosis at mossy fiber terminals in CA3 *stratum lucidum*. (A) Two-photon images from control and post-SE SpH-expressing MFBs in proximal apical dendritic region of CA3 neurons. Solid arrows indicate puncta that showed activity-driven fluorescence changes during a 600 pulse 20 Hz stimulus train. The broken arrows in the lower panel show slowly fluorescing boutons in the epileptic slices. (Scale bar = 5 μm)

(B) Representative time course of normalized fluorescence intensity of individual boutons from a control (black traces) and a post-SE (red traces) slice in response to the 600 pulse 20Hz MF stimulation (black bar shows duration of the train). **(C)** Normalized, evoked SpH fluorescence increases in response to a 600pulse 20Hz MF stimulus train, in MFBs from control (, F_{peak} = 1.47 ± 0.03, *n*=10) and post-SE (, F_{peak} = 2.02 ±0 .15, *n*=8) slices. F_{peak} was significantly increased in post-SE slices (*P*<0.05, Student's t-test; all values mean ± SEM). **(D)** Frequency distribution histogram of normalized peak SpH fluorescence for all MFB's in post-SE (F_{peak} = 1.76 ± 0.04, 100/115 puncta and 3.89 ± 0.10, 15/115 puncta) versus control (F_{peak} = 1.41 ± 0.025, 93 puncta). Inset is a cumulative histogram of normalized peak SpH fluorescence, *P*<0.001 Kolgomorov-Smirnov test. **(E)** Mean fluorescence values of scaled SpH fluorescence decay (data normalized to respective peak fluorescence values from 4C) after cessation of stimulation, control and Post-SE. Inset represents mean ± SEM of individual decay constants derived by a single exponential fit to the SpH fluorescence decay curve. Control (black bar), τ = 10.4 ± 0.77 s, *n*=67 and post-SE (red bar), τ =7.23 ± 0.32 s, *n*=133 (*, *P*<0.05, Student's t-test).

As shown in figure 4 below, we did not see any global change in VAMP-2 expression after the induction of SE. This result could be due to either a general increase in release probability of existing mossy fiber boutons or appearance of a distinct sub-population of terminals with higher release probabilities. To resolve this distinction, we plotted a distribution histogram (Figure 3D) of the normalized peak SpH fluorescence values, which are a function of the total number of vesicles released during the stimulus train. Control and post-SE distributions of peak SpH fluorescence for all individual mossy fiber boutons, indicate the appearance of a new sub-population of about 3-fold higher release rate MFBs in the post-SE animals. The cumulative probability distribution (Figure 3D inset) showed a significant increase in peak SpH fluorescence attained for the post-SE when compared to controls, *P*<0.001 Kolgomorov-Smirnov test).

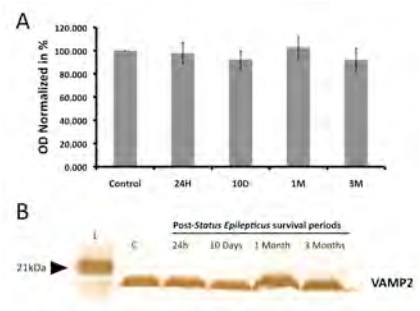

Figure 4: Western blot analysis of Synaptobrevin/VAMP2 expression after pilocarpine-induced *status epilepticus* (SE). **(A)** Graph representing semi-quantitative analysis of optical density (OD) for the synaptobrevin/VAMP2-positive bands revealed no significant differences among experimental groups (animals sacrificed at 24h, 10 days, 1 month and 3 months after SE) and control samples (data was normalized to control values and represented as bars=means ± SE, P>0.05, ANOVA n=3). **(B)** Representative Western blot experiment showing no apparent changes in the intensity of VAMP2-positive immunobands around 10-13kD for the different samples. C= Control. Ladder (L) indicates the molecular weight of 21 KDa.

Vesicular Endocytosis: To determine whether there are also changes in rate of vesicle *endocytosis* (recovery of vesicles for reuse after release) in mossy fiber boutons, we used the decay kinetics of SpH fluorescence after the end of the stimulus train. Since vesicle endocytosis is the rate-limiting step for decay in vesicle fluorescence (Sankaranarayanan and Ryan, 2000), determining the decay constant (τ) of this fluorescence gives an estimate of the rate of vesicle endocytosis. We first normalized the mean peak stimulus-evoked SpH fluorescence increases to 1.0 for control and post-SE slices, to compare directly the time courses of decay. As shown in figure 3E, the mean rate of decay of SpH fluorescence from peak to baseline for epileptic slices was significantly faster (red circles) when compared to control (black circles, *P*<0.05, Student's t-test), indicating an enhanced speed of endocytosis. We also fit single exponential decay functions to curves for individual mossy fiber boutons to determine the decay time constants in post-SE and control mossy fiber boutons. As shown in figure 3E inset above, chronic post-SE led to a significant decrease in decay time constants (red bar, τ =7.23 ± 0.32 s vs. control slices (black bar), τ =10.4 ± 0.77 s, *P*<0.05; Student's t-test) also consistent with acceleration in the rate of vesicle retrieval.

FM1-43 measurement of changes in vesicular release from the rat mossy fiber bouton readily releasable pool at early and late time points post-status epilepticus

As a second, independent measure of vesicular release, we estimated the time course of neurotransmitter release in slices from post-SE Sprague-Dawley rats using two-photon imaging of stimulus-evoked release of the styryl dye FM1-43 as described previously (Stanton *et al.*, 2003; Zakharenko *et al.*, 2003; Stanton *et al.*, 2005; Winterer *et al.*, 2006; Bailey *et al.*, 2008). We loaded FM1-43 selectively into vesicles of the RRP with a 30 sec hypertonic shock and similar to SpH fluorescence, we visualized bright puncta in the proximal region of field CA3 >2 µm in diameter (Fig. 5A, solid arrows), presumably mossy fiber boutons (Galimberti *et al.*, 2006). It is postulated hypertonic solution produces $Ca2^{+}$ independent, asynchronous release of synaptic vesicles likely due to perturbations in the tension of the interacting membranes (synaptic vesicle membrane and the plasma membrane) that leads to a decrease energy barrier for membrane fusion (Stevens and Williams, 2000). More distal puncta (Fig. 5A, white rectangular box) that took up FM1-43 were much smaller in size and likely the associational-commissural synaptic terminals. Dye release was triggered by repetitive bursts of 50 mossy fiber stimuli at a frequency of 20Hz, spaced 30 sec apart (Fig. 5B), to allow binding and clearance by the scavenger ADVASEP-7 (100 µM; Zakharenko *et al.*, 2003) and minimize potential movement artifacts.

Figure 5C shows mean time courses of RRP loaded stimulus-evoked FM1-43 destaining from mossy fiber boutons in slices up to 2 months (filled circles) post-SE was associated with a significantly enhanced release of FM1-43 (~64% from prestimulus baseline, filled red circles, when compared to age matched controls (~51% from prestimulus baseline, filled black circles, $P<0.05$, Student's t-test). Interestingly, 11 months post-SE showed a substantial slowing in MFB release rate in the epileptic group (~21% from prestimulus baseline, open red circles) versus aged matched controls (~37% of baseline, open black circles, $P<0.05$, Student's t-test).

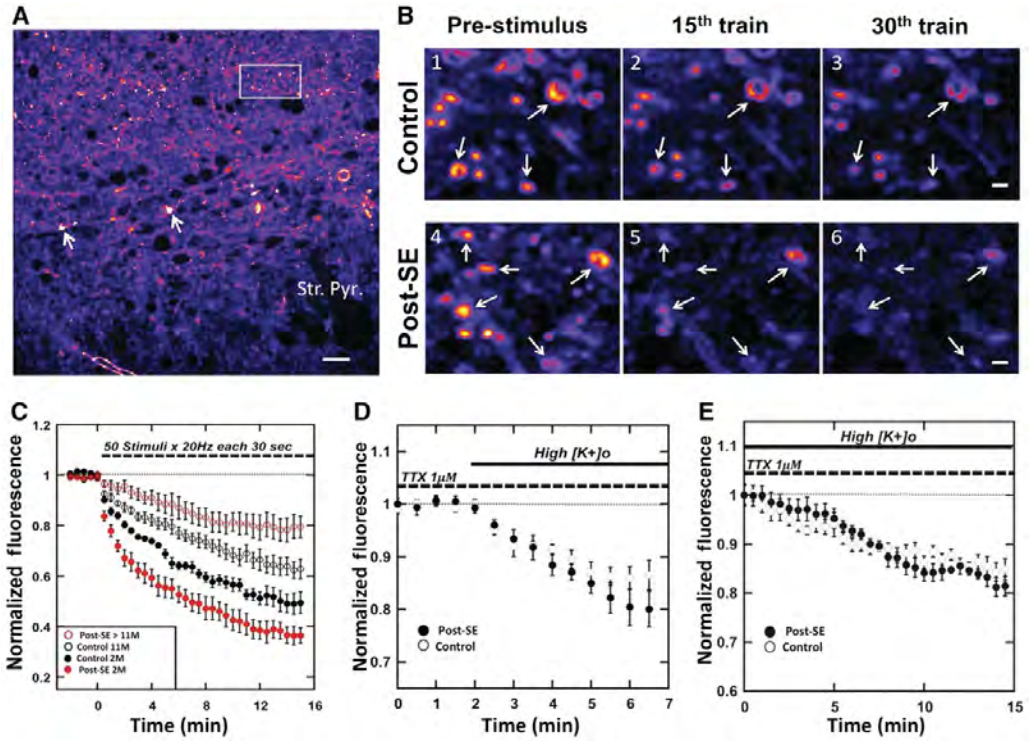

Figure 5: Pilocarpine-induced SE enhances evoked, but not action potential independent, presynaptic vesicular release of FM1-43 from the RRP in MFBs. **(A)** Two-photon image of a control field CA3 showing FM1-43 loaded RRP of MFBs. The solid arrows show staining of giant mossy fiber terminals, in the proximal region of CA3 stratum lucidum. The rectangular box outlines FM1-43 staining of puncta distal to the CA3 pyramidal cell bodies and much smaller in size, likely to be the associational-commissural synapses. Scale bar = 20 µm. **(B)** Representative time-lapse images of FM1-43 decay from the RRP using repetitive mossy fiber stimulus bursts (50 stimuli/20Hz each 30s) to evoke release from MFB in control and 2 month post-SE slices, respectively. Panels 1 and 4 illustrate pre-stimulus baseline

fluorescence, panels 2 and 5 fluorescence intensity after 15 trains, and panels 3 and 6 fluorescence intensity after 30 trains of mossy fiber stimulation. Solid arrows indicate ROI's >2 µm in diameter that showed robust stimulus dependent FM1-43 destaining. Scale bar = 10 µm **(C)** Time course of FM1-43 destaining 1-2months (2M) post-SE slices (, 0.36 ± 0.03, *n*=6), aged matched controls (, 0.49 ± 0.04, *n*=5), >11 month (11M) post-SE slices (, 0.79 ± 0.04, *n*=5) and aged matched controls (, 0.62 ± 0.04, *n*=6). (All points are mean ± SEM of normalized fluorescence decay at 30th stimulus burst). *P*<0.05, Student's t-test. **(D)** Time course of first 4.5 minutes of action potential independent FM1-43 destaining in presence of TTX (1 µM) and 15 mM [K+]o from the RRP in MFBs of 2M post-SE (filled circles, *n*=4) and aged matched control (open circles, *n*=5) slices (All points are mean ± SEM). Decay after 4.5 minutes in high [K+]o: Control = 0.86 ± 0.028 (~14% of prestimulus baseline) and post-SE = 0.80 ± 0.034 (~20% of prestimulus baseline; *P*>0.20, Student's t-test) **(E)** Late phase of spontaneous release: Time course of renormalized spontaneous FM1-43 destaining after 10-25 minutes in *High[K+]o.* Control decay = 0.85 ± 0.02 and post-SE decay = 0.81 ± 0.02 (*P*>0.20, Student's t-test, all points are mean ± SEM).

Action potential-independent release of FM1-43 is not altered by pilocarpine induced status epilepticus in rats

The above data suggests that changes in stimulus-evoked, but not necessarily spontaneous release rate in the post-SE state. To measure presynaptic spontaneous release from the RRP, we loaded FM1-43 by hypertonic shock (800 mOsm/20 s), followed by bath application of tetrodotoxin (TTX 1 µM), and extracellular [K^+] raised to 15 mM [K^+]o (*High [K+]o)* to facilitate action potential-independent release (Axmacher *et al.*, 2004). To mark the early phase of action potential-independent release, we monitored magnitude of FM1-43 destaining within the first 4.5 minutes of *High [K+]o* application (Fig. 5D), which showed no significant difference between control (~15%) and post-SE (~20%) mossy fiber boutons *(P*>0.20, Student's t-test). To determine whether steady-state spontaneous release was altered, we examined the late phase of spontaneous release 10-25 minutes after application of *High [K+]o* (Figure 5E). As in the early phase, there was no significant difference between the two groups after 25 minutes of *High [K+]o,* indicating action potential dependent and independent vesicular release from the RRP may be differentially regulated in the post-SE state.

Vesicle endocytosis becomes dynamin-independent after pilocarpine induced status epilepticus

Clathrin mediated endocytosis is the dominant mode of vesicle retrieval after synaptic vesicle endocytosis. The adaptor protein AP2, initiates the clathrin coat formation and helps recruits clathrin and the accessory protein amphiphysin to the site of endocytosis. Amphiphysin then recruits dynamin, a guanosine triphosphatase that is required for mediating membrane scission via GTP hydrolysis (Gundelfinger *et al.*, 2003). It has been demonstrated that dynamin-1 (a neuron specific dynamin) is required during intense neuronal activity (Ferguson *et al.*, 2007). Interestingly, it was recently reported that mice with a homozygous missense mutation in dynamin-1 exhibit lethal seizures, ataxia and neurosensory deficits, while the heterozygous condition leads to the occurrence of spontaneous recurrent seizures (Boumil *et al.*, 2010). To determine if pilocarpine treated post-SE animals show altered sensitivity to dynamin inhibition, we measured SpH responses from mossy fiber terminals from control and post-SE slices that were incubated with dynasore (150-200µM), a highly specific, cell-permeable inhibitor of dynamin GTPase capable of arresting clathrin-mediated endocytosis (Macia *et al.*, 2006; Newton *et al.*, 2006; Chung *et al.*, 2010), while not affecting vesicle exocytosis (Newton *et al.*, 2006). As shown in Figure 6 below, SpH fluorescence decay after cessation of stimulation was inhibited by dynasore treatment in control slices, suggesting a block in vesicle endocytosis (Newton et al., 2006). Interestingly there was a significant increase in the peak SpH fluorescence attained in the presence of dynasore. This is likely due to an unmasking of endocytosis that occurs during the stimulation train (Newton *et al.*, 2006; Chung *et al.*, 2010). However dynasore treatment of post-SE slices showed no increase in the peak fluorescence during the stimulus train, although there was an inhibition in the decay of SpH fluorescence after the end of the stimulation train.

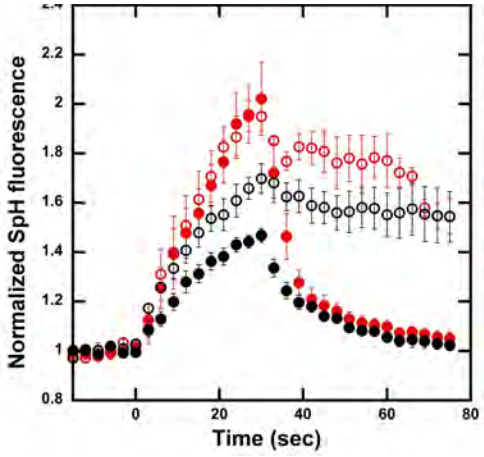

Figure 6: Differential effect of dynamin inhibition on vesicular recycling in control vs epileptic animals. Slices were pre-incubated with dynasore 150-200µM for 45minutes prior to and during image acquisition. Black filled circles represent control normalized SpH responses (with peak fluorescence at 1.4 ± 0.03 of baseline) to a 20Hz/600 stimulation train in the absence of dynasore, while the black empty circles represent a significant increase in the peak normalized SpH responses (1.7 ± 0.06, P<0.05) to 20Hz/600 stimulation in the presence of dynasore. Red filled circle represent control SpH responses to a 20Hz/600 stimulation train in the absence of dynasore leading to normalized peak fluorescence at 2.02 ± 0.15, while in the presence of dynasore (red empty circles) there was no significant increase in the normalized peak SpH fluorescence 1.95 ± 0.05) in response to a 20Hz/600 stimulation, P> 0.05.

The lack of this boost in vesicle exocytosis during the stimulation train in the epileptic tissue could be because of an alteration in dynamin expression. To test this hypothesis, we immunoblotted extracts from hippocampal lysates with antibodies that recognize, dynamin1,2,3 (pan dynamin) or the individual isoforms of dynamin-1 or 2. As shown in figure 7A, a significant increase in pan dynamin expression was seen 24 hour, 10 days, 1 month and 3 months post-SE when compared to age matched control. There was however no difference detected in dynamin-1 or dynamin-2 expression alone. Additionally there was increase (~19.5%) in expression of Ser774 phosphorylated dynamin 1-3 (p-Dynamin) in 3-4 months epileptic rats vs controls (Figure 7C-D, Student's t-test, P<0.05). This could affect the interaction of dynamin with binding partners such as syndapin I and could alter synaptic vesicle endocytosis (Anggono *et al.*, 2006).

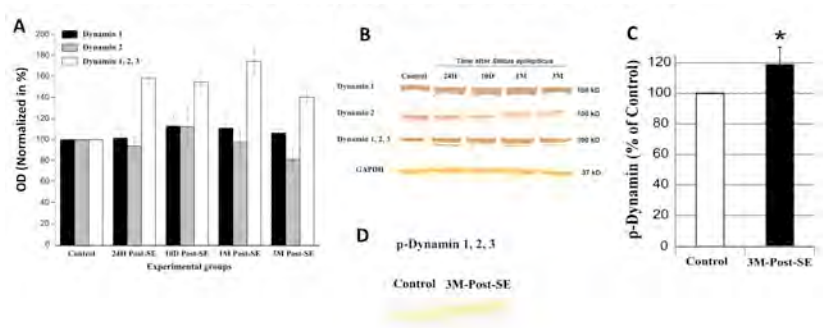

Figure 7: Western immunoblot analysis for Dynamin expression in hippocampal lysates (A) from control rats and rats sacrificed at 24 hour, 10 days, 30–60 days (1 month) and 3 months post-SE. Bars represent mean optical density (OD) index normalized to control values. Semi-quantitative OD analysis of bands revealed a significant increase in pan Dyanmin expression (1-3) after SE (*one-way ANOVA, F =8.07, p < 0.0001* and HSD post-hoc *p<0.05*). (**B)** Representative immunoblots for Dynamin 1, 2 and pan Dynamin. GAPDH was used as loading control. **(C)** Increased (~19.5%) expression of Ser774 phosphorylated Dynamin 1-3 (p-Dynamin) in 3-4 months epileptic rats vs controls (Student t-test, p <0.05). **(D)** Immunoblot of p-Dynamin.

Our results show that, in the first 1-2 months post-SE, morphological changes develop in the mossy fiber bouton cytoarchitecture, and are correlated with both an increase in vesiclular release rate of mossy fiber boutons and appearance of a high release rate sub-population. At late stages post-seizure (11 months), a time when substantial postsynaptic neuronal damage has occurred in hippocampal field CA3 (hippocampal sclerosis), transmitter release is markedly reduced, a potentially compensatory mechanism which, nevertheless, does not seem to prevent continued spontaneous seizures, and which will undoubtedly have important negative consequences for cognition and memory.

In a recent manuscript published in the high profile journal Brain (Upreti et al., 2012; 5-year Impact Factor 10.143, ranked 12th of 265 neuroscience journals; see appendix), we described the epilepsy-associated long-term alterations in presynaptic morphology and synaptic vesicle recycling we discovered at mossy fiber-CA3 terminals of mice and rats subjected to pilocarpine-induced SE, a seizure model that produces a chronic epileptic state associated with spontaneous generalized seizures in 100% of animals (Muller et al., 2009). We found increases in 1) mossy fiber bouton (MFB) size, 2) number of release sites per MFB, 3) number of RRP and RP vesicles, 4) active zone length, 5) action potential-driven vesicular release rate measured with either FM1-43 or SpH-expressing transgenic mice, and 6) vesicle endocytosis. These alterations persisted for 3 months following a single sustained SE, making it likely they are important contributors to development and maintenance of the epileptic state.

YEAR 01 Garrido Lab

Task 2. Evaluate the effects of different concentrations of "classical" (e.g. carbamazepine and topiramate), and "new generation" antiepileptic drugs (e.g. LEV) on patch-clamp electrophysiological recordings from dentate granule cells that give rise to mossy fibers. This data will be used to assess the effects of antiepileptic drugs on spontaneous miniature excitatory postsynaptic currents (mEPSC) in control versus pilocarpine treated rats. (To be accomplished in the laboratory of Dr. Garrido-Sanabria)

- **Subtask 2a.** Develop chronic epileptic rats with a single injection of pilocarpine (Dr. Garrido and Dr. Pacheco; months 1-12).
- **Subtask 2b.** Prepare hippocampal slices from control and epileptic rats (Dr. Garrido and Dr. Pacheco; months 1-12).
- **Subtask 2c.** Perform patch-clamp recordings from granule cells to record spontaneous mEPSCs (Dr. Garrido and Dr. Pacheco; months 1-12).
- **Subtask 2d.** Test whether antiepileptic drugs modify frequency and amplitude of mEPSCs in granule cells in control versus epileptic rats (Dr. Garrido and Dr. Pacheco; months 1-12).
- **Subtask 2c.** Statistical analysis of data (Dr. Garrido and Dr. Pacheco, months 9-12).

YEAR 02

Specific Aim 2: *Assess whether antiepileptic drugs acting on presynaptic sites can reduce or prevent seizure induced long-term potentiation of vesicular release from mossy fiber boutons in MTLE.*

Working hypothesis: Epileptic rats exhibit enhanced pool size and release probability from the rapidly-recycling vesicle pool, and SV2a down-regulation contributes to this enhanced release. Chronic treatment with LEV or other presynaptic antiepileptic drugs during epileptogenesis is predicted to protect presynaptic function and normal glutamate release, and perhaps reduce, or even prevent, seizures **(months 13-24).**

YEAR 03

Specific Aim 3: *Assess whether down-regulation of mGluR2 and SV2a at mossy fiber terminals can be reversed by chronic treatment with presynaptic antiepileptic drugs* (months 25-36).

Working hypothesis: Reduced expression of SV2A and mGluR2 results in deficient mGluR2-mediated suppression of presynaptic release and reduced anticonvulsant efficacy of LEV. To evaluate the role of altered mGluR2 and SV2a expression epilepsy, we will perform patch-clamp recordings from granule cells in control and pilocarpine-treated epileptic rats and investigate the effects of LEV and mGluR2 agonists and antagonists on the amplitude and frequency of spontaneous EPSCs. Functional data will be correlated with changes in gene expression of mGluR2 and SV2A in dissected CA3 and dentate gyrus regions **(months 24-36).**

KEY RESEARCH ACCOMPLISHMENTS:

- Established and optimized the pilocarpine model of chronic epilepsy in our laboratory for both rats and synaptopHluorin-expressing transgenic mice
- Comprehensive characterization of the baseline properties of presynaptic vesicular release from control mossy fiber terminals in hippocampal slices from both rats and synaptopHluorin-expressing transgenic mice
- Discovery that pilocarpine epilepsy is associated, 1-2 months post-seizures, with marked increases in the size of hippocampal mossy fiber terminals and the appearance of ectopic boutons that synapse in a layer of field CA3 where they do not normally synapse.
- Discovery that the appearance of these larger boutons correlates with marked increases in vesicular release from mossy fiber terminals and the appearance of a population of very high release rate boutons in both rats and SpH-expressing mice 1-2 months post-seizure.
- Discovery that, in addition to exocytosis, endocytotic vesicle recycling is also persistently enhanced 1-2 months following pilocarpine-induced seizures.
- Discovery that down-regulation of dynamin may be a key component in seizure-induced shifts in endocytotic recycling pathways and properties.
- Publication in the high impact journal *Brain* of our study of pilocarpine-induced long-lasting morphological and functional alterations in mossy fiber terminals in both rats and SpH-expressing mice.
- Established the pilocarpine epilepsy model in SV2A knockout mice acquired from Dr. Garrido-Sanabria at UTB.
- Commenced studies using 2-photon laser scanning microscopy to evaluate the effects of levetiracetam, carbamezipine, lamotrigine and topiramate on presynaptic vesicular release in control versus pilocarpine-seized epileptic rats and SpH mice.

REPORTABLE OUTCOMES:

Manuscripts

1) Manuscript published in *Brain* (2012; see Appendix), Journal Impact Factor 10.143

Upreti C, Otero R, Partida C, Skinner F, Thakker R, Pacheco LF, Zhou ZY, Maglakelidze G, Velíšková J, Velíšek L, Romanovicz D, Jones T, **Stanton PK,** Garrido-Sanabria ER (2012) Altered neurotransmitter release, vesicle recycling and presynaptic structure in the pilocarpine model of temporal lobe epilepsy. *Brain* 135 (Pt 3): 869-885.

Data from this grant was presented in 4 scientific meetings in 2011 (below) and new data will be presented at the Society for Neuroscience meeting in 2012.

National Meetings

1) Data from electrophysiological and pharmacological experiments was submitted to the Society for Neuroscience Meeting that will be held October 13 - 17, 2012, in New Orleans, LA. E. G. Sanabria, L. F. Pacheco, L. M. Rambo, J. M. Rodriguez, C. Upreti, **P. K. Stanton**. Levetiracetam inhibits excitatory drive onto dentate gyrus granule cells: Effects of SV2A gene dosage and pilocarpine-induced epilepsy. (see Abstract in Appendix).

2) Upreti C, Skinner F, Otero R, Thakker R, Rosas G, Partida C, Pacheco LF, Jones TA, Romanovicz D, **Stanton PK** and Garrido-Sanabria ER. Abnormal function and reorganization of presynaptic nanocomponents in experimental epilepsy: A multiphoton laser scanning confocal imaging and transmission electron microscopy study. *3rd Meeting of the American Society for Nanomedicine,* Rockville, MD, Nov 9-11, 2011.

3) Upreti C, **Stanton PK,** Garrido-Sanabria ER. Abnormalities in presynaptic vesicle pools of mossy fiber boutons in the pilocarpine model of mesial temporal lobe epilepsy. Poster. 779.10/Z13 *Society for Neuroscience Meeting*, Washington, Nov 16, 2011.

4) Upreti C, Garrido-Sanabria ER, **Stanton PK**. Abnormal functional and ultrastructural changes of synaptic vesicle pools at active zones in mossy fiber boutons in mesial temporal lobe epilepsy, (ID: 1149994), presented at the *65th America Epilepsy Society Annual Meeting*, Baltimore, December 2-6, 2011.

5) Garrido-Sanabria ER, Otero R, Thakker R, Partida C, Skinner F, Jones T, Romanovicz D, Upreti C, **Stanton PK.** Abnormal Ultrastructure of Large Mossy Fiber Boutons-CA3 pyramidal Cell Synapses in Mesial Temporal Lobe Epilepsy. (ID: 1150094), presented at the *65th America Epilepsy Society Annual Meeting*, Baltimore, December, 2011.

CONCLUSION

In year 01, we completed the majority of our studies in Aim 1 and a portion of Aim 2. We found that severe pilocarpine-induced seizures that result in long-term appearance of spontaneous epileptic seizures are associated with marked changes in the structure of hippocampal mossy fiber presynaptic terminals and functional hyperexcitability of presynaptic vesicular transmitter release. Mossy fiber terminals were greatly increased in size, as was the size of the transmitter release active zone and readily-releasable vesicle pool, and there was even sprouting of new mossy fiber terminals into the stratum oriens layer of field CA3 where such terminals do not normally synapse. Functionally, these presynaptic glutamatergic terminals showed greatly enhanced rate of vesicular release from the rapidly-recycling vesicle pool and accelerated endocytotic recycling of vesicles back into this vesicle pool. We showed these functional changes in both rats and mice, using two different fluorescent indicators to image, by 2-photon laser scanning microscopy, individual mossy fiber release sites in the hippocampal CA3 field. We commenced studies which will be completed in year 02 to test the ability of four antiepileptic drugs that act via differing mechanisms (levetiracetam, lamotrigine, carbamezipine and topiramate), to control presynaptic vesicular release two months after pilocarpine-induced seizures, when the brain has become spontaneously epileptic. We also discovered that the presynaptic vesicle protein dynamin, which is an essential component of one vesicle recycling pathway, is markedly down-regulated in expression and the dynamin pathway loses its ability to keep up with vesicular release in the epileptic brain.

Recommended change: While we have now begun implementing the pilocarpine seizure model in transgenic mice where the vesicle protein SV2A has been knocked out, we plan to determine whether a loss of SV2A and dynamin interaction might be responsible for seizure-induced enhancement in glutamate release, by examining the ability of the dynamin-inhibiting peptide dynasore to alter recycling in SV2A knockout versus wild-type mice.

Significance: While all but one antiepileptic drug acts by modifying postsynaptic neuronal excitability, our work indicates that extensive changes in presynaptic function are also associated with epilepsy. Increases in glutamate release, while certainly able to contribute to hyperexcitation in seizures, also have the potential to damage and even kill their postsynaptic target neurons. If we can find agents that can control presynaptic release, and do so even after development of epilepsy when release is enhanced, we would have a whole new class of treatments to help the 40% of epileptic patients who do not respond to any current therapeutics. Understanding the mechanisms by which seizures change presynaptic function is the essential first step towards this goal.

REFERENCES

Acsady L, Kamondi A, Sik A, Freund T, Buzsaki G. GABAergic cells are the major postsynaptic targets of mossy fibers in the rat hippocampus. J Neurosci. 1998 May 1;18(9):3386-403.

Anggono V, Smillie KJ, Graham ME, Valova VA, Cousin MA, Robinson PJ. Syndapin I is the phosphorylation-regulated dynamin I partner in synaptic vesicle endocytosis. Nat Neurosci. 2006 Jun;9(6):752-60.

Bailey CP, Nicholls RE, Zhang XL, Zhou ZY, Muller W, Kandel ER, et al. Galpha(i2) inhibition of adenylate cyclase regulates presynaptic activity and unmasks cGMP-dependent long-term depression at Schaffer collateral-CA1 hippocampal synapses. Learn Mem. 2008;15(4):261-70.

Bayazitov IT, Richardson RJ, Fricke RG, Zakharenko SS. Slow presynaptic and fast postsynaptic components of compound long-term potentiation. J Neurosci. 2007 Oct 24;27(43):11510-21.

Blackstad TW, Brink K, Hem J, Jeune B. Distribution of hippocampal mossy fibers in the rat. An experimental study with silver impregnation methods. J Comp Neurol. 1970 Apr;138(4):433-49.

Boulland, J.L.*, et al.* Changes in vesicular transporters for gamma-aminobutyric acid and glutamate reveal vulnerability and reorganization of hippocampal neurons following pilocarpine-induced seizures. *J Comp Neurol* **503**, 466-485 (2007).

Boumil RM, Letts VA, Roberts MC, Lenz C, Mahaffey CL, Zhang ZW, et al. A missense mutation in a highly conserved alternate exon of dynamin-1 causes epilepsy in fitful mice. PLoS Genet. 2010 Aug;6(8).

Burrone J, Li Z, Murthy VN. Studying vesicle cycling in presynaptic terminals using the genetically encoded probe synaptopHluorin. Nat Protoc. 2006;1(6):2970-8.

Chung C, Barylko B, Leitz J, Liu X, Kavalali ET. Acute dynamin inhibition dissects synaptic vesicle recycling pathways that drive spontaneous and evoked neurotransmission. J Neurosci. 2010 Jan 27;30(4):1363-76.

Claiborne BJ, Amaral DG, Cowan WM. A light and electron microscopic analysis of the mossy fibers of the rat dentate gyrus. J Comp Neurol. 1986 Apr 22;246(4):435-58.

Danzer SC, He X, Loepke AW, McNamara JO. Structural plasticity of dentate granule cell mossy fibers during the development of limbic epilepsy. Hippocampus. 2010 Jan;20(1):113-24.

Epsztein, J., Represa, A., Jorquera, I., Ben-Ari, Y. & Crepel, V. Recurrent mossy fibers establish aberrant kainate receptor-operated synapses on granule cells from epileptic rats. *J Neurosci* **25**, 8229-8239 (2005).

Esclapez, M., Hirsch, J.C., Ben-Ari, Y. & Bernard, C. Newly formed excitatory pathways provide a substrate for hyperexcitability in experimental temporal lobe epilepsy. *J Comp Neurol* **408**, 449-460 (1999).

Ferguson SM, Brasnjo G, Hayashi M, Wolfel M, Collesi C, Giovedi S, et al. A selective activity-dependent requirement for dynamin 1 in synaptic vesicle endocytosis. Science. 2007 Apr 27;316(5824):570-4.

Galimberti I, Gogolla N, Alberi S, Santos AF, Muller D, Caroni P. Long-term rearrangements of hippocampal mossy fiber terminal connectivity in the adult regulated by experience. Neuron. 2006 Jun 1;50(5):749-63.

Gundelfinger ED, Kessels MM, Qualmann B. Temporal and spatial coordination of exocytosis and endocytosis. Nat Rev Mol Cell Biol. 2003 Feb;4(2):127-39.

Li Z, Burrone J, Tyler WJ, Hartman KN, Albeanu DF, Murthy VN. Synaptic vesicle recycling studied in transgenic mice expressing synaptopHluorin. Proc Natl Acad Sci U S A. 2005 Apr 26;102(17):6131-6.

Macia E, Ehrlich M, Massol R, Boucrot E, Brunner C, Kirchhausen T. Dynasore, a cell-permeable inhibitor of dynamin. Dev Cell. 2006 Jun;10(6):839-50.

Mello, L.E.*, et al.* Circuit mechanisms of seizures in the pilocarpine model of chronic epilepsy: cell loss and mossy fiber sprouting. *Epilepsia* **34**, 985-995 (1993).

Miesenbock G, De Angelis DA, Rothman JE. Visualizing secretion and synaptic transmission with pH-sensitive green fluorescent proteins. Nature. 1998 Jul 9;394(6689):192-5.

Muller, C.J., Bankstahl, M., Groticke, I. & Loscher, W. Pilocarpine vs. lithium-pilocarpine for induction of status epilepticus in mice: development of spontaneous seizures, behavioral alterations and neuronal damage. *Eur J Pharmacol* **619**, 15-24 (2009).

Newton AJ, Kirchhausen T, Murthy VN. Inhibition of dynamin completely blocks compensatory synaptic vesicle endocytosis. Proc Natl Acad Sci U S A. 2006 Nov 21;103(47):17955-60.

Pacheco Otalora, L.F., Couoh, J., Shigamoto, R., Zarei, M.M. & Garrido Sanabria, E.R. Abnormal mGluR2/3 expression in the perforant path termination zones and mossy fibers of chronically epileptic rats. *Brain Res* **1098**, 170-185 (2006).

Sankaranarayanan S, Ryan TA. Real-time measurements of vesicle-SNARE recycling in synapses of the central nervous system. Nat Cell Biol. 2000 Apr;2(4):197-204.

Schauwecker, P.E. Strain differences in seizure-induced cell death following pilocarpine-induced status epilepticus. *Neurobiol Dis* **45**, 297-304 (2012).

Stanton PK, Winterer J, Bailey CP, Kyrozis A, Raginov I, Laube G, et al. Long-term depression of presynaptic release from the readily releasable vesicle pool induced by NMDA receptor-dependent retrograde nitric oxide. J Neurosci. 2003 Jul 2;23(13):5936-44.

Stanton PK, Winterer J, Zhang XL, Muller W. Imaging LTP of presynaptic release of FM1-43 from the rapidly recycling vesicle pool of Schaffer collateral-CA1 synapses in rat hippocampal slices. Eur J Neurosci. 2005 Nov;22(10):2451-61.

Stevens CF, Williams JH. "Kiss and run" exocytosis at hippocampal synapses. Proc Natl Acad Sci U S A. 2000 Nov 7;97(23):12828-33.

Turski WA, Cavalheiro EA, Bortolotto ZA, Mello LM, Schwarz M, Turski L. Seizures produced by pilocarpine in mice: a behavioral, electroencephalographic and morphological analysis. Brain Res. 1984 Nov 12;321(2):237-53.

Upreti, C*,* Otero R, Partida C, Skinner F, Thakker R, Pacheco L, Zhou ZY, Maglakelidze GM, Velíšková J, Velíšek L, Romanovicz D, Jones T, **Stanton PK,** and Garrido-Sanabria ER (2012) Altered neurotransmitter release, vesicle recycling and presynaptic structure in the pilocarpine model of temporal lobe epilepsy. *Brain* **135**, 869-885 (2012).

Winterer J, Stanton PK, Muller W. Direct monitoring of vesicular release and uptake in brain slices by multiphoton excitation of the styryl FM 1-43. Biotechniques. 2006 Mar;40(3):343-51.

Zakharenko SS, Zablow L, Siegelbaum SA. Altered presynaptic vesicle release and cycling during mGluR-dependent LTD. Neuron. 2002 Sep 12;35(6):1099-110.

APPENDIX

1) Upreti, C, Otero R, Partida C, Skinner F, Thakker R, Pacheco L, Zhou ZY, Maglakelidze GM, Velíšková J, Velíšek L, Romanovicz D, Jones T, **Stanton PK,** and Garrido-Sanabria ER (2012) Altered neurotransmitter release, vesicle recycling and presynaptic structure in the pilocarpine model of temporal lobe epilepsy. *Brain* **135**, 869-885 (2012).

2) Sanabria EG, Pacheco LF, Rambo LM, Rodriguez JM, Upreti C and **Stanton PK** (2012) Levetiracetam inhibits excitatory drive onto dentate gyrus granule cells: Effects of SV2A gene dosage and pilocarpine-induced epilepsy. *Society for Neuroscience 42nd Annual Meeting,* in press.

Brain Advance Access published February 16, 2012

BRAIN
A JOURNAL OF NEUROLOGY

Altered neurotransmitter release, vesicle recycling and presynaptic structure in the pilocarpine model of temporal lobe epilepsy

Chirag Upreti,[1] Rafael Otero,[2] Carlos Partida,[2] Frank Skinner,[2] Ravi Thakker,[2] Luis F. Pacheco,[2] Zhen-yu Zhou,[1] Giorgi Maglakelidze,[1] Jana Velíšková,[1,3] Libor Velíšek,[1,4] Dwight Romanovicz,[5] Theresa Jones,[6] Patric K. Stanton[1,7] and Emilio R. Garrido-Sanabria[2]

1 Department of Cell Biology and Anatomy, New York Medical College, Valhalla, NY 10595, USA
2 Department of Biomedicine, University of Texas Brownsville, Brownsville, TX 78520, USA
3 Department of Obstetrics and Gynaecology, New York Medical College, Valhalla, NY 10595, USA
4 Department of Paediatrics, New York Medical College, Valhalla, NY 10595, USA
5 Institute for Cellular and Molecular Biology, University of Texas Austin, Austin, TX 78712, USA
6 Department of Psychology, Institute for Neuroscience, University of Texas Austin, Austin, TX 78712, USA
7 Department of Neurology, New York Medical College, Valhalla, NY 10595, USA

Correspondence to: Emilio R. Garrido-Sanabria, MD, PhD,
Epilepsy Research Laboratory,
Department of Biomedicine,
University of Texas Brownsville,
80 Fort Brown, BRHP 2117,
Brownsville,
TX 78520, USA
E-mail: emilio.garrido@utb.edu

In searching for persistent seizure-induced alterations in brain function that might be causally related to epilepsy, presynaptic transmitter release has relatively been neglected. To measure directly the long-term effects of pilocarpine-induced status epilepticus on vesicular release and recycling in hippocampal mossy fibre presynaptic boutons, we used (i) two-photon imaging of FM1-43 vesicular release in rat hippocampal slices; and (ii) transgenic mice expressing the genetically encoded pH-sensitive fluorescent reporter synaptopHluorin preferentially at glutamatergic synapses. In this study we found that, 1–2 months after pilocarpine-induced status epilepticus, there were significant increases in mossy fibre bouton size, faster rates of action potential-driven vesicular release and endocytosis. We also analysed the ultrastructure of rat mossy fibre boutons using transmission electron microscopy. Pilocarpine-induced status epilepticus led to a significant increase in the number of release sites, active zone length, postsynaptic density area and number of vesicles in the readily releasable and recycling pools, all correlated with increased release probability. Our data show that presynaptic release machinery is persistently altered in structure and function by status epilepticus, which could contribute to the development of the chronic epileptic state and may represent a potential new target for antiepileptic therapies.

Keywords: epilepsy; neurotransmitter release; hippocampus; synaptic vesicle recycling; mossy fibre terminals

Abbreviations: MFB = mossy fibre bouton; RRP = readily releasable pool; SpH = SynaptopHluorin

Received August 10, 2011. Revised October 4, 2011. Accepted November 8, 2011.

Introduction

Hippocampal mossy fibres exhibit complex structural rearrangements and abnormal synaptic function in mesial temporal lobe epilepsy (McNamara, 1994; Frotscher *et al.*, 2006; Dudek and Sutula, 2007; Danzer *et al.*, 2010). During epileptogenesis, axons of dentate gyrus granule cells sprout and establish abnormal excitatory synapses onto multiple targets, including granule cells, interneurons and CA3 pyramidal neurons (McNamara, 1994; Wenzel *et al.*, 2000; Frotscher *et al.*, 2006; Dudek and Sutula, 2007). While studies have shown alterations in postsynaptic function of excitatory and inhibitory circuits in mesial temporal lobe epilepsy (Coulter, 2000; Gorter *et al.*, 2002), far less attention has been paid to presynaptic dysfunction in the pathogenesis of epilepsy.

Large mossy fibre boutons (MFBs) have multiple release sites with substantial numbers of small and large clear synaptic vesicles containing glutamate (Chicurel and Harris, 1992; Rollenhagen *et al.*, 2007). Large synaptic vesicles are thought to mediate the monoquantal nature of 'giant' miniature excitatory postsynaptic currents onto CA3 pyramidal cells, allowing action potential invasion of presynaptic MFBs to trigger neurotransmitter release in amounts that reliably excite CA3 pyramidal neurons. During status epilepticus, excessive glutamate release from MFBs can be highly deleterious to survival of CA3 neurons and is thought to be responsible for the massive and sustained neuronal damage in the CA3 region (Zhang *et al.*, 2009).

Surprisingly little is known about the long-term effects of status epilepticus on vesicular release of transmitter from MFBs. Goussakov *et al.* (2000) found that, several weeks after kainic acid-induced status epilepticus, mossy fibre, but not associational-commissural, synapses exhibit impaired induction of long-term potentiation, markedly reduced paired-pulse facilitation and augmentation of burst induced mossy fibre-CA3 excitatory field potential (Goussakov *et al.*, 2000). These changes in activity-dependent plasticity were also associated with a significant increase in the size of the readily releasable pool (RRP) of vesicles, suggesting a persistent increase in release probability at mossy fibre–CA3 synapses (Goussakov *et al.*, 2000). Ultrastructural features and targets of abnormally sprouted MFBs in the inner molecular layer have been studied by electron microscopy in models of mesial temporal lobe epilepsy (Cavazos *et al.*, 2003; Frotscher *et al.*, 2006); indeed, redistribution of synaptic vesicles to a 'strategic position' in the vicinity of the synaptic cleft has been described after kindled seizures (Hovorka *et al.*, 1989), but these studies did not characterize the arrangement of active zones and morphological features of vesicle pools.

We used the cholinergic agonist pilocarpine to induce prolonged status epilepticus as a model of mesial temporal lobe epilepsy (Turski *et al.*, 1984; Curia *et al.*, 2008), to test the hypothesis that status epilepticus can result in long-term enhancement of vesicular release from MFBs. Assessing presynaptic release properties by patch-clamp electrophysiology in long-term epileptic animals is hampered by the CA3 pyramidal neurons being susceptible to cell death due to excitotoxicity, thus are not optimal to record from as biosensors of transmitter release. Here we utilized two different methods to directly image presynaptic vesicular release by using two-photon laser scanning microscopy of (i) the styryl dye FM1-43 (Pyle *et al.*, 1999), which selectively labels transmitter vesicles for direct visualization of destaining kinetics, in slices from control versus post-status epilepticus rats; and (ii) imaging exocytosis–endocytosis kinetics from individual MFBs in acute hippocampal slices from transgenic mice that selectively express the pH-sensitive vesicle fusion protein synaptopHluorin (SpH) (Li *et al.*, 2005). We also used transmission electron microscopy of rat hippocampus to investigate whether the post-status epilepticus period is associated with ultrastructural modifications at active zones of MFBs in the stratum lucidum correlated with functional changes in vesicular release (Dobrunz and Stevens, 1997; Murthy *et al.*, 1997; Schikorski and Stevens, 1997; Matz *et al.*, 2010).

By each of these measures, we found a persistent enhancement of vesicular release, vesicle endocytosis and ultrastructure reorganization of active zones in MFBs after status epilepticus. These changes are likely to add to observed changes in intrinsic excitability of granule cells and circuit plasticity to increase the excitatory drive from granule cells onto CA3 pyramidal neurons in MTLE.

Materials and methods

Experiments were performed in accordance with the National Institutes of Health Guidelines for the Care and Use of Laboratory Animals as approved by New York Medical College and University of Texas Brownsville Institutional Animal Care and Use Committees.

Pilocarpine-induced status epilepticus

Status epilepticus was induced by a single pilocarpine intraperitoneal injection (350 mg/kg in saline) to 30- to 35-day-old Sprague–Dawley rats (Taconic) or SpH21 mice (C57BL/6J background, kind gift from Dr Venkatesh Murthy, Harvard University) following standard procedures (Cavalheiro, 1995; Pacheco *et al.*, 2008). Animals received methylscopolamine nitrate (0.1 mg/kg in saline, subcutaneous) 30 min before pilocarpine to minimize peripheral effects of cholinergic stimulation (Turski *et al.*, 1984). Rats seized for 3 h, mice 1 h (Muller *et al.*, 2009), and motor seizures were terminated with one diazepam injection (10 mg/kg in saline, intraperitoneal). Only animals experiencing continuous status epilepticus during these periods were studied. Controls animals received methylscopolamine and saline instead of pilocarpine.

Hippocampal slice preparation and electrophysiological recordings

Rats and mice 1–2 months post-status epilepticus and age-matched controls were decapitated under deep isoflurane anaesthesia, their brains quickly removed, hemisected in ice-cold sucrose-based cutting solution (Bischofberger *et al.*, 2006) in mM: 87 NaCl, 25 $NaHCO_3$, 25 glucose, 75 sucrose, 2.5 KCl, 1.25 NaH_2PO_4, 0.5 $CaCl_2$ and 7 $MgCl_2$ (equilibrated with 95% O_2/5% CO_2), and 350–400 μm thick horizontal hippocampal slices cut with a vibratome (DSK model

DTK-1000). Slices were submerged in cutting solution at 32°C for 30 min, then transferred to a holding chamber in room temperature artificial CSF (in mM: 126 NaCl, 3 KCl, 1.25 NaH_2PO_4, 1.3 MgCl, 2.5 $CaCl_2$, 26 $NaHCO_3$, 10 glucose) saturated with 95% O_2/5% CO_2. Evoked field excitatory postsynaptic potentials were recorded in the proximal dendritic field in stratum lucidum for at least 15 min before starting an experiment.

Two-photon laser scanning microscopy

Fluorescence was visualized with a customized two-photon laser-scanning Olympus BX61WI microscope with a ×60/0.90 NA water immersion infrared objective lens and an Olympus multispectral confocal laser scan unit. The light source was a Mai-Tai^{TM} laser (Solid-State Laser Co.), tuned to 825 nm for exciting Alexa Fluor 594, and 890 nm for exciting SpH and FM1-43. Epifluorescence was detected with photomultiplier tubes of the confocal laser scan head with pinhole maximally open and emission spectral window optimized for signal over background. A 565-nm dichroic mirror (Chroma Technology) separated green and red fluorescence to eliminate transmitted or reflected excitation light. Depending on the fluorophore, HQ525/50 (SpH) or HQ605/50 (FM1-43 or Alexa Fluor 594) filters were placed in the 'green' pathways. Images were acquired with Fluoview FV300 software (Olympus America). Although there were no signs of photodamage, we used the lowest intensity needed for adequate signal-to-noise ratios. Pixel images (512 × 512) were acquired, 0.15 μm/pixel in $x-y$ axes and, in some cases, 8–10 μm steps of 0.5–1 μm in the z-axis. For imaging MFBs, glass microelectrodes with broken tips ($R < 1$ MΩ) were dipped in 1% Alexa Fluor 594 10-kDa dextran (Invitrogen) in distilled water until the tip filled by capillarity action, desiccated for 2–3 days until dye formed a crystal particle at the tip. During the experiment, dye coated tips (with sealed backends) were inserted ~50–100 μm into the dentate gyrus granule cell layer for 15–20 min, then slices were transferred to a holding chamber in artificial CSF at 32°C for 30 min, followed by room temperature for 1–1.5 h, before imaging. Using NIH ImageJ, greyscale images of Alexa Fluor 594 filled MFBs flanked by at least one axonal process were processed by automated Otsu thresholding to eliminate investigator bias (Lee *et al.*, 2011), and cross-sectional area of binary images measured. A total of 8–10 images were acquired in a z-axis stack in 0.2–0.5 μm steps for 3D reconstruction (Supplementary Video 3). For SpH fluorescence experiments, slices were perfused with 25 μM 6-cyano-7-nitroquinoxaline-2,3-dione (CNQX; Tocris) and 50 μM D-(-)-2-Amino-5-phosphonopentanoic acid (D-AP5; Tocris). A 600 stimulus 20-Hz train in the stratum lucidum evoked SpH fluorescence increases (imaged within 100 μm from stimulating electrode) in the proximal region (the first 100 μm) of CA3 apical dendrites and images were acquired every 30 s. While extracellular brain pH changes during seizures, first to alkaline and later to acidic (Xiong and Stringer, 2000), we use SpH as a pH-sensitive indicator of vesicular release in brain slices bathed in artificial CSF (containing 25 μM CNQX and 50 μM D-AP5 to prevent synaptically driven action potentials and epileptiform activity) in our recording chamber with pH maintained at or ~7.4. To calculate half-time of post-stimulus decay of SpH peak fluorescence intensity, ($t_{1/2}$) was calculated for each punctum by single exponential fits to destaining curves using the equation: $y_0 + A_1e^{(-x/t_1)}$, with t_1 the decay constant. Data were analysed with OriginPro and presented with KaleidaGraph (Synergy software).

FM1-43 loading and destaining of the readily releasable vesicle pool

FM1-43 was loaded into the RRP as previously described (Stanton *et al.*, 2003, 2005). After recording a 15 min stable baseline field excitatory postsynaptic potential (~50% of maximum amplitude), 25 μM CNQX and 50 μM D-AP5 were bath applied to prevent synaptically driven action potentials and epileptiform activity from accelerating dye release or inducing synaptic plasticity. Presynaptic boutons were loaded by 5-min bath applied 5 μM FM1-43 in normal artificial CSF, followed by hypertonic artificial CSF (800 mOsm) for 30 s to load the RRP, returned to normal artificial CSF with 5 μm FM1-43 for 1 min, then washed out with dye-free artificial CSF (Supplementary Fig. 2). Stimulus-induced destaining was evoked by a 50 stimulus 20-Hz train each 30 s, and measured after 30 min in dye-free artificial CSF plus 100 μM ADVASEP-7 to scavenge and remove extracellular FM1-43. To measure spontaneous release, after FM1-43 loading, slices were continuously bathed in 1 μM tetrodotoxin, 25 μm CNQX and 50 μM D-AP5 and extracellular [K^+] raised to 15 mM [K^+]o (*High[K+]o)* to facilitate action potential-independent release (Axmacher *et al.*, 2004). For some slices, 8–10 images were acquired in 0.5–1 μm in the z-axis at each time point, maximal intensity z-axis projections were made for this subset of the final stack. Circular regions of interest were selected around centres of bright, punctate fluorescence spots at least 2 μm in diameter within 100 μm of the CA3 pyramidal cell body layer. Activity-dependent destaining time courses were generated by correcting for bleaching, subtracting background fluorescence and normalizing each region of interest to pre-stimulus intensity as previously reported (Stanton *et al.*, 2003, 2005; Tyler *et al.*, 2006). Vertical bars show SEMs for all normalized and corrected boutons.

Tissue preparation for immunohistochemistry

Age-matched control and epileptic SpH mice (<6 months post-status epilepticus) were anaesthetized with 100 mg/kg ketamine, the brain removed and immersed for 48 h in 4% formaldehyde in 0.1 M sodium phosphate buffer (pH 7.4) plus 0.9% NaCl (phosphate-buffered saline). After a phosphate-buffered saline wash, brains were cryoprotected in 30% sucrose in phosphate-buffered saline for ~48 h at 4°C, frozen in Optimum Cutting Temperature Compound (EMS Co.) at −20°C, and 40 μm thick coronal sections sliced with a cryostat (HM500 Microm, Zeiss) and stored in 150 mM Tris plus 150 mM NaCl (Tris-buffered saline; pH 7.4) and 0.1% NaN_3. Several sections were Nissl-stained to assess seizure-mediated neuronal loss and cyto-architectonic boundaries. Free-floating sections from controls and post-status epilepticus were processed simultaneously for VGluT1 and NeuN immunofluorescence as described (Pacheco *et al.*, 2008). The extent of cell loss in the CA3 subfield was assessed at ×400 magnification by using grid morphometric techniques (Gorter *et al.*, 2003). A 240 × 240 μm box was placed over the region of interest (CA3 area) and NeuN-labelled cells in the pyramidal layer, presumed neurons, were counted by an observer masked to experimental group/condition. Counts of three sections per animal were averaged. Final neuron counts were calculated as the density of neurons per 0.1 mm^2. It should be noted that this technique provides a relative estimate and not absolute calculation of the number of neurons in a region. Statistical differences in the number of neurons per square millimetre between control and pilocarpine-treated epileptic groups were

determined by Student's *t*-test with significance set at $P < 0.05$. The cross-sectional diameter of SpH-positive VGluT1-labelled puncta in the granule cell layer and supragranular region was measured in three confocal images of dentate gyrus per animal per group using the measuring tool of Fluoview (Olympus).

Fixation and embedding for transmission electron microscopy

Tissue was prepared for transmission electron microscopy using standard methods (Miranda *et al.*, 2011). Seven post-status epilepticus and six age-matched Sprague–Dawley rats were anaesthetized with ketamine (50 mg/kg, intraperitoneal injection), transcardially perfused with saline followed by fixative (2% paraformaldehyde, 2% glutaraldehyde, 0.002% $CaCl_2$ in 0.1 M cacodylate and Hank's buffered salt solution; pH 7.3–7.4), and their brains were removed, sliced in 5-mm thick slabs, and post-fixed in fresh fixative overnight at room temperature. Serial 250-μm thick sections were cut with a vibratome in Hank's buffered salt solution (1000 Plus, Vibratome Co.), and the hippocampus and surrounding cortex dissected away. Samples were osmicated in 2% buffered osmium tetroxide, a 50:50 mixture of 4% osmium tetroxide and 4% potassium ferrocyanide in 0.2 M cacodylate buffer (EMS Co.), then contrasted in 1% aqueous uranyl acetate. Tissue was flat-embedded in 50:50 Spurr/Epon (EMS Co.) and polymerized at 60°C for 24 h before resin blocks were pseudo-randomly selected and trimmed to ~1 mm^3 trapezoids containing the CA3 pyramidal cell layer and stratum lucidum. To identify field CA3, 1–2 μm sections were stained with 0.1% cresyl violet acetate solution and viewed on a transmitted light scope. Ultrathin sections (55 ± 5 nm) were cut through stratum lucidum of CA3 with a Leica Ultracut ultramicrotome and collected on Formvar-coated copper slotted grids.

Transmission electron microscopy inspection and identification of mossy fibre boutons

Images 26 000× (FEI Tecnai) were used to identify regions of interest in field CA3 containing cross-sectioned or parallel bundles of axons and large MFBs (1–5 μm diameter) with numerous synaptic vesicles. For blind analysis of morphometry, coded images were imported into NIH ImageJ. Active zones were distinguished by the following criteria: (i) synaptic vesicles in close proximity to a presynaptic density; (ii) asymmetry between pre- and postsynaptic densities; and (iii) widening of the synaptic cleft (Rollenhagen *et al.*, 2007). Asymmetric (excitatory) non-perforated synapses with well-defined presynaptic compartments, clear synaptic clefts and postsynaptic density were analysed. Perforated synapses refer to a presumably more efficacious synapse subtype found in the CNS characterized by a discontinuous postsynaptic density (Calverley and Jones, 1987; Itarat and Jones, 1992; Adkins *et al.*, 2008). The number of perforated and non-perforated synapses was compared between groups

Active zone length was measured by a continuous line following the contour of presynaptic membrane on the synaptic cleft. Synaptic cleft width was averaged from three measures of distance between pre- and postsynaptic membranes (centre and ~20 nm from cleft ends). Postsynaptic density area was measured as the contour around electron-dense aggregates and postsynaptic membrane. The active zone length and quantification of synaptic vesicles was performed in single ultrathin sections using a modified 2D cross-sectional method as described previously (Miranda *et al.*, 2011) using NIH ImageJ.

The RRP was defined as the number of synaptic vesicles <60 nm from the presynaptic membrane, and the releasable pool of vesicles 60–200 nm from the presynaptic membrane (Rollenhagen *et al.*, 2007). Docked synaptic vesicles consisted of vesicles immediately adjacent to or fused to the active zone presynaptic membrane. Perimeter and mean area of synaptic vesicles were also measured, and number of active zones exhibiting ultrastructural signs of bulk endocytosis indicative of intense synaptic activity (Meunier *et al.*, 2010).

Differences in vesicle pool size were assessed by non-parametric Kolmogorov–Smirnov two-sample test (MiniAnalysis, Synaptosoft), and differences in means of normally distributed measurements were evaluated using two-tailed Student's *t*-test. Significance level was preset to $P < 0.05$. Correlation analysis between parameters was performed with non-parametric Spearman analysis, since most parameters were not normally distributed. Correlations were classified as weak [Spearman rho (r) value < 0.40], moderate ($0.4 < r < 0.7$) and strong ($r > 0.7$).

Results

Two-photon laser scanning microscopy imaging of large mossy fibre boutons of synaptopHluorin-expressing transgenic mice in acute hippocampal slices

SpH is a fusion protein that consists of a pH-sensitive pHluorin fused to the C-terminus luminal domain of the vesicle SNARE protein synaptobrevin (Miesenbock *et al.*, 1998). Under resting conditions, the luminal pH of the synaptic vesicle is acidic (pH ~5.5), resulting in proton dependent quenching of SpH fluorescence. When vesicle exocytosis is triggered and glutamate released, the lumen of the vesicle is exposed to the more alkaline pH of the extracellular space (pH ~7.2), resulting in a 20-fold increase in SpH fluorescence. When the vesicle membrane is retrieved by endocytosis and the vesicle reformed, it undergoes rapid reacidification by the vesicular ATPase, which returns SpH to its quenched state. The SpH21 transgenic mice line we used in this study expresses SpH preferentially at glutamatergic synapses (Li *et al.*, 2005; Burrone *et al.*, 2006; Bayazitov *et al.*, 2007). A representative two-photon laser scanning image of the CA3 region of an acute hippocampal slice from this mouse (Fig. 1A) contains bright GFP-positive boutons >2 μm in diameter, proximal to CA3 pyramidal cell bodies in the region innervated by mossy fibre axons of dentate granule cells (Blackstad *et al.*, 1970; Claiborne *et al.*, 1986). Associational-commissural CA3 synapses were significantly smaller (<1 μm in diameter) and more distal to our region of interest (rectangular box, Fig. 1A).

To independently confirm that large SpH expressing boutons were mossy fibre terminals, we used anterograde, bulk labelling of mossy fibres with Alexa Fluor 594 dextran introduced into the granule cell layer of the dentate gyrus (Fig. 1B). During a 1.5- to 2-h incubation, Alexa Fluor 594 dextran was taken up by granule cells and transported anterogradely to label mossy fibre axons and presynaptic boutons (Fig. 1C, Supplementary Fig. 1A and Supplementary Video 3). Figure 1E and F illustrate that some

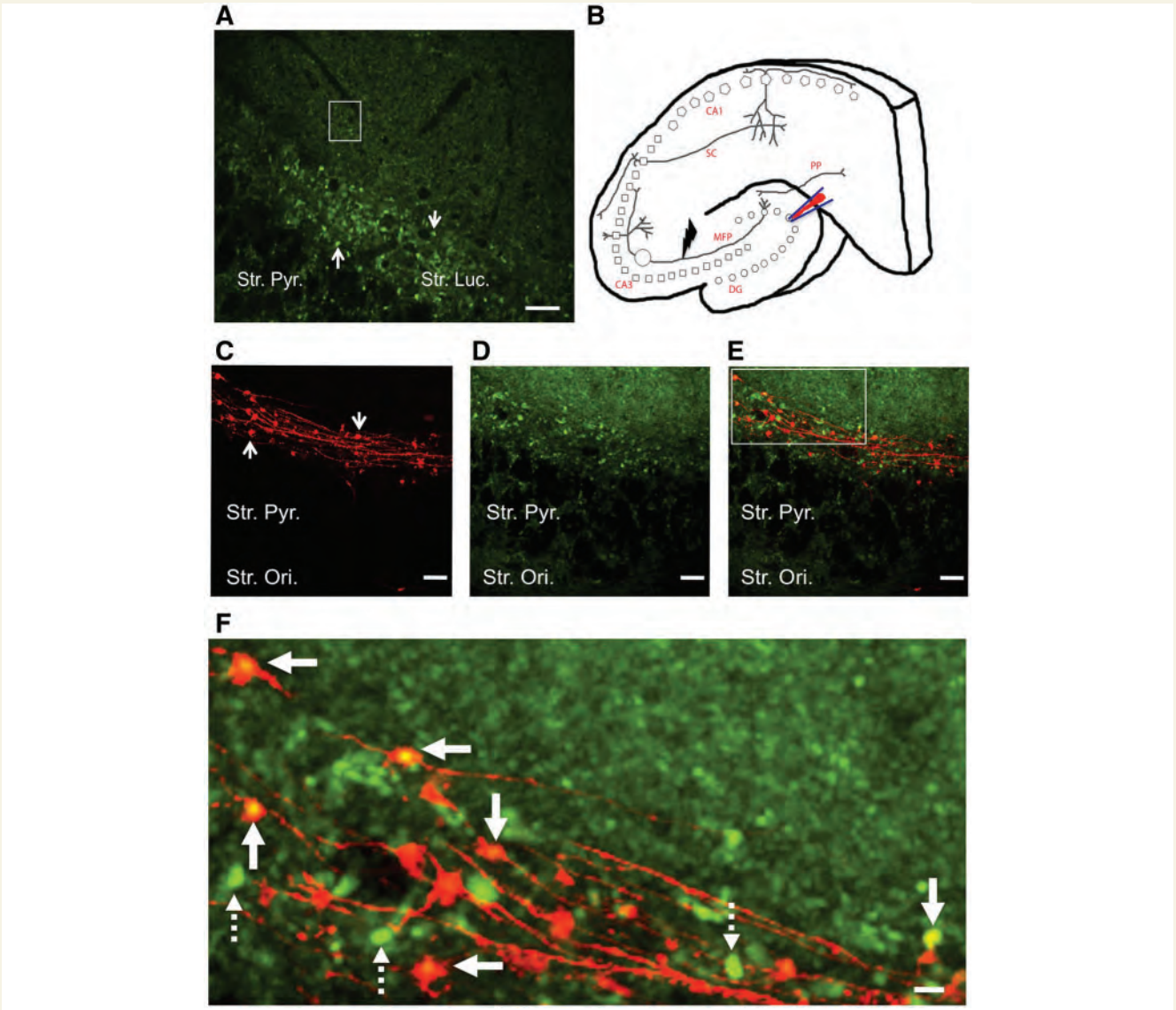

Figure 1 Visualizing MFBs in acute hippocampal slices from SpH21 transgenic mice. (**A**) Live cell two-photon laser scanning image of field CA3 of SpH-expressing glutamatergic terminals in a control hippocampal slice (post natal 60 days of age). The arrows depict representative fluorescence puncta (~4–5 μm in diameter) in the proximal (stratum lucidum, Str. Luc.) region of CA3 pyramidal cells (seen here as a ghost layer) that are likely to be giant MFBs. Distal puncta shown within the rectangular box are notably smaller in size and likely represent associational-commissural synapses in stratum radiatum. (**B**) Schematic representing hippocampal circuitry with the circle in the mossy fibre pathway (MFP) depicting the area of imaging Lightning symbol depicts the area of local stimulation and the pipette in the dentate granule cell layer (DG) showing the area of Alexa Fluor 594 dextra containing pipette insertion. Squares and pentagons depict CA3 and CA1 pyramidal cell layers, respectively. (**C**) Alexa Fluor 594 dextran filled mossy fibre axons and giant MFBs (arrows) showing characteristic *en-passant* arrangement along the axonal projections, visualized using 825 nm excitation. (**D**) Same region as (**C**) but visualized with 890-nm excitation to see SpH native fluorescence. CA3 pyramidal cell bodies can be seen as ghost cells in stratum pyramidal, and bright giant MFBs in stratum lucidum. (**E–F**) Merged images of (**C**) and (**D**) showing co-localization (**F**: arrows) between SpH and Alexa Fluor 594 dextran-labelled puncta. (**F**) Digital zoom of image from the inset box in (**E**). Note not all SpH-positive puncta co-localize with Alexa Fluor 594 puncta (broken arrows). PP = perforant path; SC = Schaffer collaterals; Str. Ori. = stratum oriens; Str. Pyr. = stratum pyramidale. Scale bars: **A** = 20 μm; **C–E** = 20 μm; and **F** = 4 μm.

(solid arrows) but not all (broken arrows) SpH and Alexa Fluor 594-positive boutons were co-labelled confirming that the large (>2 μm in diameter) SpH fluorescent puncta within the proximal 60 μm of the CA3 cell body are excitatory MFBs (Fig. 1D). Incomplete co-localization is likely because Alexa Fluor 594 labelled a subset of mossy fibre axons in stratum lucidum, along with sparse SpH expression in the excitatory terminals (Li *et al.*, 2005; Burrone *et al.*, 2006).

Pilocarpine-induced status epilepticus causes disorganization of dentate gyrus and CA3 cytoarchitecture in synaptopHluorin-expressing transgenic mice

In the hippocampal CA3 region of both control and post-status epilepticus mice (Fig. 2A), immunostaining for the presynaptic glutamate transporter VGluT1 was intense in the mossy fibre projection area in stratum lucidum, where it co-localized with native SpH fluorescence, consistent with the glutamatergic nature of presynaptic terminals expressing SpH in SpH21 mice (Li *et al.*, 2005; Burrone *et al.*, 2006). There was also ~51% reduction in CA3 stratum pyramidale of post-status epilepticus mice in the density of neurons (117.9 ± 35.4 cells/0.1 mm^2, $n = 6$, Student's *t*-test, $P < 0.01$, Fig. 2A), consistent with seizure-induced loss of CA3 pyramidal neurons following pilocarpine-induced status epilepticus reported previously (Mello *et al.*, 1993; Schauwecker, 2012).

In the dentate gyrus, we detected robust SpH fluorescence in the inner molecular layer and hilus of both control and post-status epilepticus mice (Fig. 2B), closely co-localized with VGluT1 immunofluorescence (Fig. 2B). VGluT1 puncta positive for SpH fluorescence in the inner molecular layer exhibited 39.5% larger cross-sectional diameters (Fig. 2B, 1.84 ± 0.54 µm, Student's *t*-test, $P < 0.001$) and 47.5% higher normalized mean fluorescence intensity (Fig. 2B, post-status epilepticus: VGluT1) relative to background-subtracted baseline intensity [204.8 ± 35.5 arbitrary units (a.u), $n = 29$, Student's *t*-test, $P < 0.0001$] in pilocarpine-treated post-status epilepticus mice compared with controls (Fig. 2B, control: VGluT1 138.8 ± 32.2 a.u and mean diameter of puncta: 1.31 ± 0.37 µm, $n = 29$). Interestingly, SpH puncta in granule cell somata in the control dentate gyri exhibited little immunostaining for VGluT1, whereas the granule cell layers of post-status epilepticus hippocampi showed strong co-immunolabelling for VGluT1 (Fig. 2B), suggesting either a possible upregulation of VGluT1 expression in existing terminals or neo-synaptogenesis manifested by the appearance of ectopic glutamatergic (VGluT1 positive) terminals in both inner molecular and granule cell layers during epileptogenesis, as previously reported in animal models of MTLE (Mello *et al.*, 1993; Esclapez *et al.*, 1999; Epsztein *et al.*, 2005; Pacheco *et al.*, 2006; Boulland *et al.*, 2007).

Pilocarpine-induced status epilepticus persistently increases size and vesicular release rate of mossy fibre boutons in synaptopHluorin-expressing mice

Live cell imaging of MFBs in acute hippocampal slices was done by bulk loading a group of granule cells and their axons with Alexa Fluor 594-dextran. Dye-filled excrescences (Fig. 1B) were classified as the main body of giant MFBs if they had at least a 4 µm^2 cross-sectional area (Claiborne *et al.*, 1986; Acsady *et al.*, 1998; Danzer *et al.*, 2010). The mean area of MFBs 1–2 months after pilocarpine induced-status epilepticus was significantly enhanced (~21.09%, Fig. 3C, $P = 0.008$, Mann–Whitney U-test, $n = 7$) compared with aged matched controls ($n = 7$). A frequency distribution histogram of individual MFBs from epileptic animals revealed a significant rightward shift in the curves (Fig. 3B; $P < 0.05$, Kolmogorov–Smirnov test), consistent with increased MFB volumes.

To determine whether post-status epilepticus leads to functional differences in transmitter release from excitatory MFBs, we utilized two-photon live cell imaging in slices from SpH21 mice. To trigger vesicular release from MFBs in CA3 stratum lucidum (Fig. 1B–F), granule cell axons in slices from control and post-status epilepticus animals were stimulated with a single, continuous train of 600 stimuli at 20 Hz (Fig. 1B and Supplementary Video 4A and B, respectively), a paradigm that recruits both the RRP and rapidly recycling vesicle pools (Li *et al.*, 2005). Representative time-lapse images (Fig. 4A) of control and post-status epilepticus SpH-expressing MFBs showed robust, cumulative increases in SpH fluorescence intensity during the stimulus train, followed by return of fluorescence to baseline levels ~40 s after stimulus termination. Figure 4C plots the normalized mean SpH fluorescence responses in control versus post-status epilepticus animals, which showed significantly larger stimulus-evoked rises in SpH fluorescence (2.02 ± 0.15, red circles, $n = 8$, $P < 0.05$, Student's *t*-test) compared with controls (1.47 ± 0.03, black circles, $n = 10$).

This result could be due to either a general increase in release probability of existing MFBs or appearance of a distinct sub-population of terminals with higher release probabilities. To resolve this distinction, we plotted a distribution histogram (Fig. 4D) of the normalized peak SpH fluorescence values, which is a function of the total number of vesicles released during the stimulus train. Control and post-status epilepticus distributions of peak SpH fluorescence for all individual MFBs indicate the appearance of a new sub-population of ~3-fold higher release rate MFBs in the post-status epilepticus animals. The cumulative probability distribution (Fig. 4D inset) showed a significant increase in peak SpH fluorescence attained for the post-status epilepticus MFBs compared with controls ($P < 0.001$, Kolmogorov–Smirnov test).

Taken together, these results suggest that, in the first 1–2 months post-status epilepticus, morphological changes develop in the MFB cytoarchitecture, correlated with both an increase in vesicular release rate of MFBs and appearance of a high release rate sub-population of terminals.

Pilocarpine-induced status epilepticus persistently enhances vesicular endocytosis in mossy fibre boutons of synaptopHluorin-expressing mice

To determine whether there are changes in rate of vesicle endocytosis in MFBs, we used the decay kinetics of SpH fluorescence after the end of the stimulus train. Since vesicle endocytosis is the rate-limiting step for decay in vesicle fluorescence (Sankaranarayanan and Ryan, 2000), determining the decay constant (τ) of this fluorescence gives an estimate of the rate of

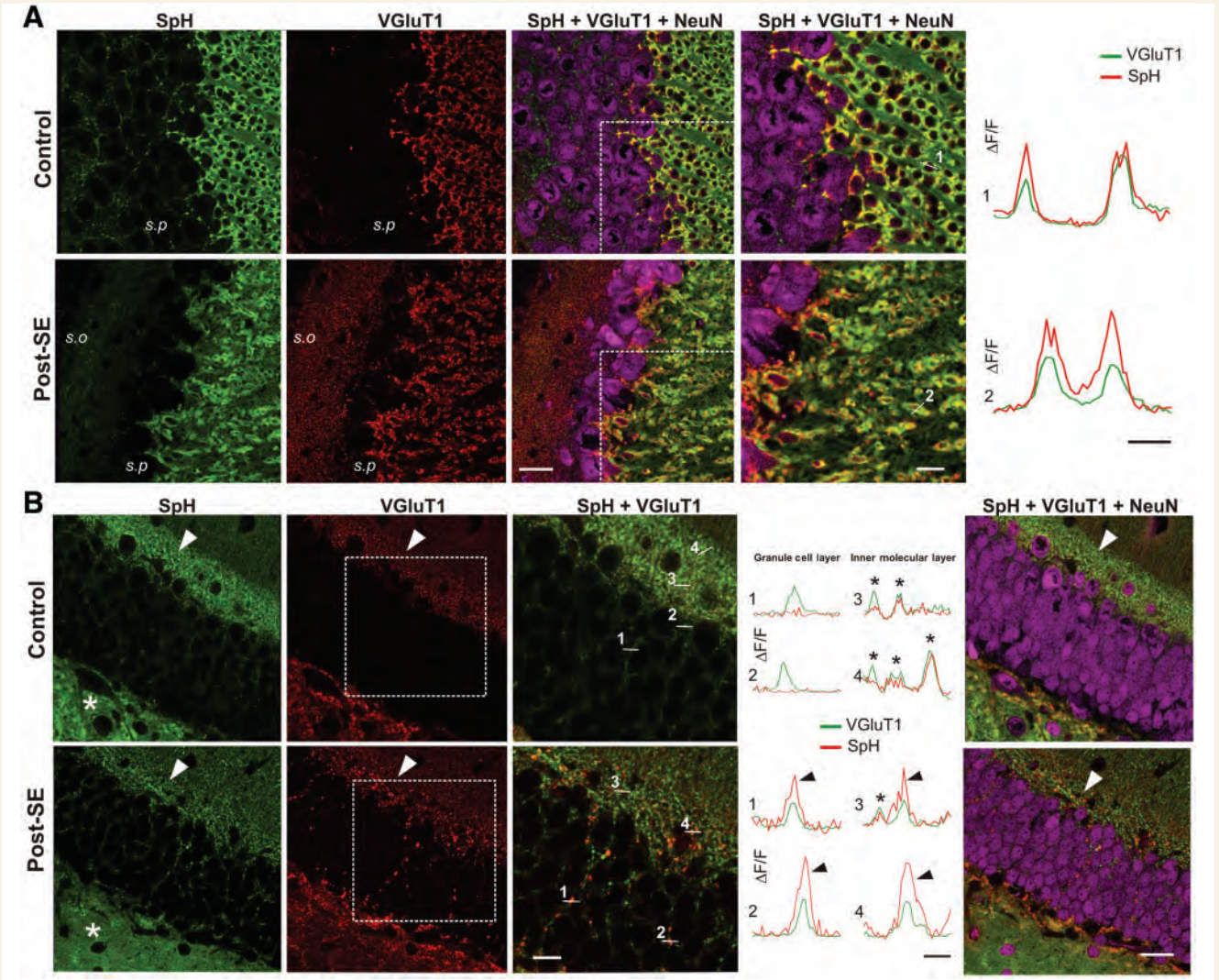

Figure 2 Confocal images of SpH, VGluT1 and NeuN expression in CA3 (**A**) and dentate granule cell (**B**) layers of control and post-status epilepticus (SE) SpH transgenic mice. (**A**) Native SpH fluorescence image (green), VGluT1 immunofluorescence image (red) and NeuN immunofluorescence image (purple) in control and post-status epilepticus mice showing co-localization of SpH with VgluT1 labelling in MFBs. A dramatic loss of cells was noticed in CA3 stratum pyramidale by NeuN staining (SpH + VGluT1 + NeuN, column 3) and SpH and VGluT1-positive terminals appear disorganized in stratum lucidum of post-status epilepticus compared with controls (SpH + VGluT1 + NeuN, column 4). Punctate SpH signals were also scattered through the pyramidal cell layer (s.p) surrounding cell somata that were stained with NeuN antibody. The column on the *right* (column 4) shows fluorescence intensity profile and co-localization along line scans (1: control and 2: post-status epilepticus) through single MFBs indicated in the respective ×2 magnification images (scale bar = 25 μm) of the rectangular boxes seen in column 3 (scale bar = 50 μm). Scale bar for line scans = 2 μm. (**B**) In the dentate granule cell layer of control and post-status epilepticus, (NeuN labelling), SpH fluorescence (green) and VGluT1 immunofluorescence (red) were intense in the hilus (asterisk) and in the inner molecular layer (arrow head). In the control (**B,** *top* row) SpH-positive puncta around putative granule cell somata were devoid of VGluT1 expression (line plots: lines 1 and 2), while SpH and VGluT1 signals co-localized in the inner molecular layer (line plots: lines 3 and 4), as shown by respective line scans of fluorescence intensity through puncta in the granule cell layer (1 and 2) versus the inner molecular layer (3 and 4). In post-status epilepticus (**B,** *bottom* row) SpH and VGluT1 co-localize in both the dentate granule cell layer (SpH + VGluT1) and inner molecular layer. NeuN immunofluorescence illustrates a lack of marked granule cell loss in post-status epilepticus dentate gyrus (SpH + VGluT1 + NeuN). Stratum oriens scale bar = 2 μm.

vesicle endocytosis. We first normalized the mean peak stimulus-evoked SpH fluorescence increases to 1.0 for control and post-status epilepticus slices, to compare directly the time courses of decay. As shown in Fig. 4E, the mean rate of decay of SpH fluorescence from peak to baseline for epileptic slices was significantly faster (red circles) compared with control slices (black circles, $P < 0.05$, Student's *t*-test), indicating an enhanced speed of endocytosis. We also fit single exponential decay functions to curves for individual MFBs to determine the decay time constants in post-status epilepticus vs. control MFBs. As shown in the Fig. 4E inset, chronic post-status epilepticus led to a significant decrease in decay time constants [red bar, $\tau = 7.23 \pm 0.32$ s versus

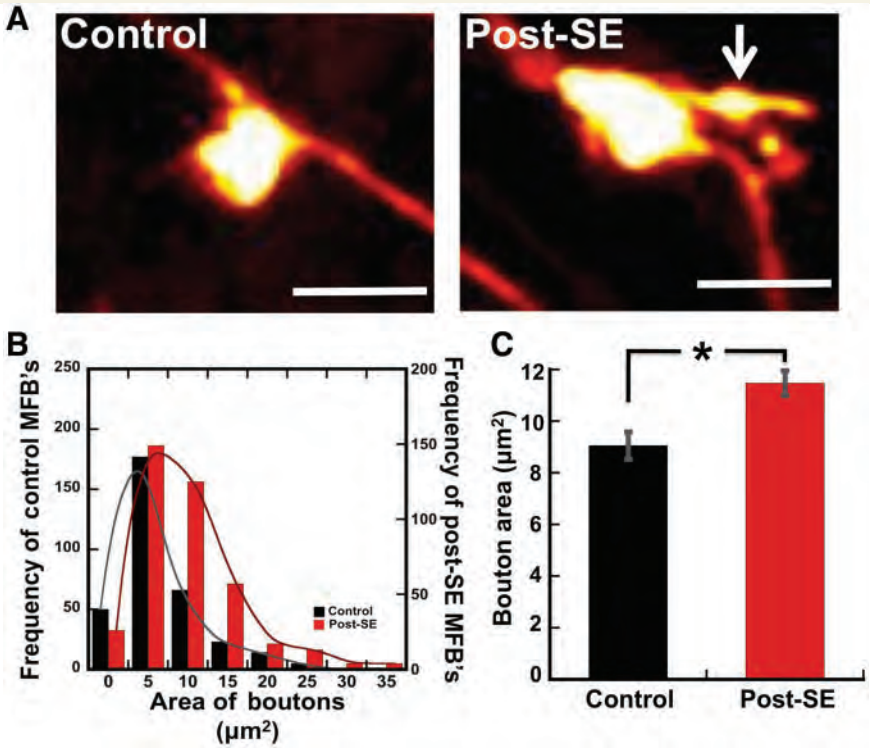

Figure 3 Pilocarpine-induced status epilepticus (SE) leads to persistent increases in dentate gyrus giant MFB area. (**A**) Live cell two-photon images of Alexa Fluor 594 dextran-loaded giant mossy fibre terminals from field CA3 of acute hippocampal slices from control and post-status epilepticus mice. The arrow shows a filopodia-like projection arising from the giant MFB. (**B**) Frequency distribution histogram of individual MFB areas from control (black columns, total of 336 boutons, $n = 7$) vs. 1–2 months post-SE mice (red columns, 394 boutons, $n = 7$). (**C**) Mean MFB area for control (black column, $9.05 \pm 0.52\ \mu m^2$) and epileptic (red column, $11.47 \pm 0.48\ \mu m^2$) mice. Data plotted as mean ± SEM, $^*P < 0.05$, Mann–Whitney U-test. Scale bar **A** = 5 μm.

control slices (black bar), $\tau = 10.4 \pm 0.77$ s, $P < 0.05$; Student's *t*-test] also consistent with acceleration in the rate of vesicle retrieval.

FM1-43 measurement of changes in vesicular release from the rat mossy fibre bouton readily releasable pool at early and late time points post-status epilepticus

As a second, independent measure of vesicular release, we estimated the time course of neurotransmitter release in slices from post-status epilepticus Sprague–Dawley rats using two-photon imaging of stimulus-evoked release of the styryl dye FM1-43 as described previously (Stanton *et al.*, 2003, 2005; Zakharenko *et al.*, 2003; Winterer *et al.*, 2006; Bailey *et al.*, 2008). We loaded FM1-43 selectively into vesicles of the RRP with a 30-s hypertonic shock (Supplementary Fig. 2) and similar to SpH fluorescence, we visualized bright puncta in the proximal region of field CA3 > 2 μm in diameter (Fig. 5A), presumed MFBs (Galimberti *et al.*, 2006). More distal puncta that took up FM1-43 were much smaller in size, consistent with associational-commissural synaptic terminals. Dye release was triggered by repetitive bursts of 50 mossy fibre stimuli at a frequency of 20 Hz, spaced 30 s apart (Fig. 5B and Supplementary Fig. 2), to allow binding and clearance by the scavenger ADVASEP-7 (100 μm) (Zakharenko *et al.*, 2003) and minimize potential movement artefacts.

Figure 5C shows that mean time courses of RRP loaded stimulus-evoked FM1-43 destaining from MFBs in slices up to 2 months post-status epilepticus was associated with a significantly enhanced release of FM1-43 (~64% from pre-stimulus baseline), when compared with age matched controls (~51% from pre-stimulus baseline, $P < 0.05$, Student's *t*-test). Interestingly, 11 months post-status epilepticus rats showed a substantial slowing in MFBs release rate in the epileptic group (~21% from pre-stimulus baseline) versus aged matched controls (~37% of baseline, $P < 0.05$, Student's *t*-test).

Action potential-independent release of FM1-43 from the mossy fibre bouton readily releasable pool is not persistently altered by pilocarpine-induced status epilepticus in rats

The above data suggest changes in stimulus evoked, but not necessarily spontaneous release rate post-status epilepticus.

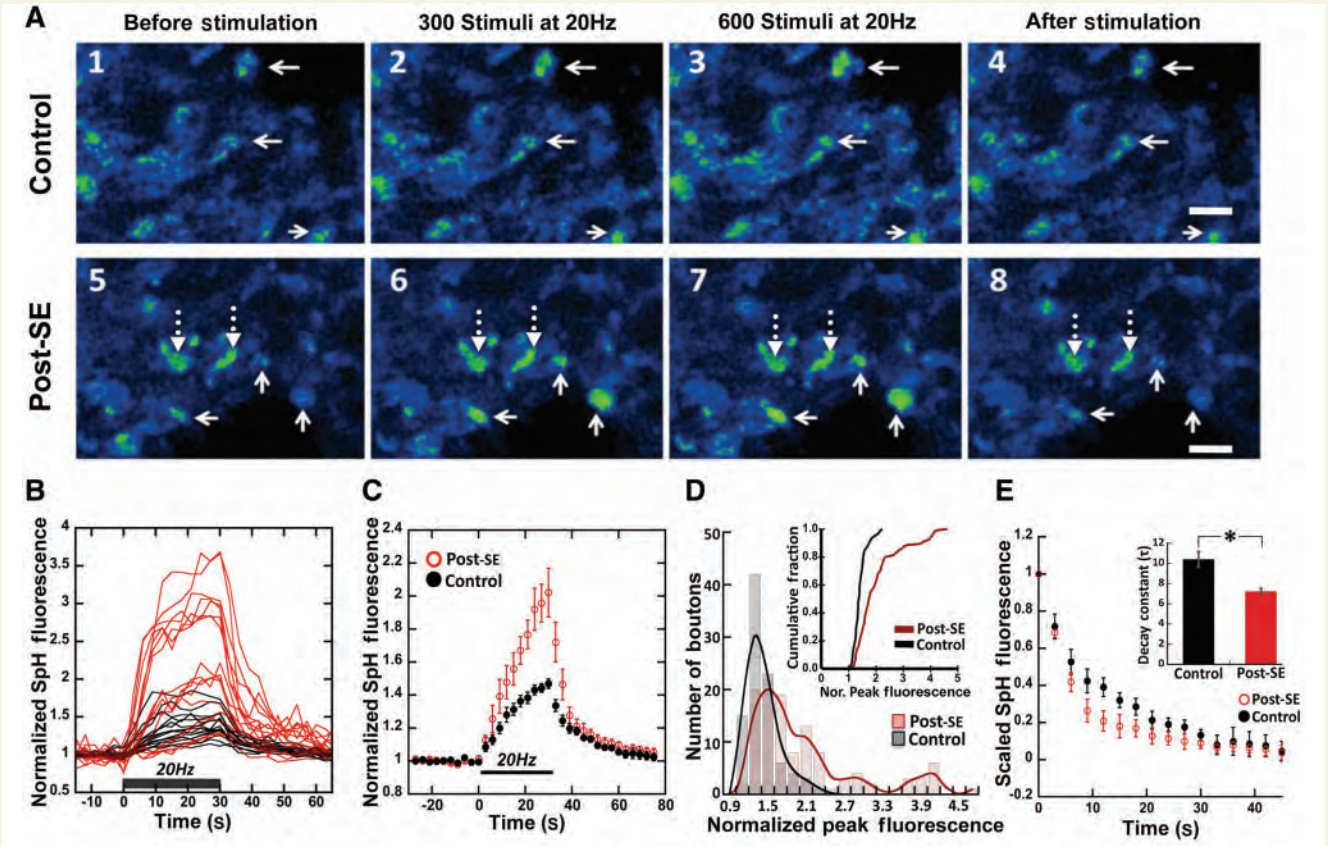

Figure 4 Pilocarpine-induced status epilepticus (SE) enhances vesicular release and endocytosis at mossy fibre terminals in CA3 stratum lucidum. (**A**) Time-lapse two-photon images from control and post-status epilepticus SpH-expressing MFBs in the proximal apical dendritic region of field CA3. Solid arrows indicate puncta that showed activity-dependent fluorescence changes during a 600 pulse/20 Hz stimulus train. The broken arrows in (**A**, *bottom* row) show there were some slowly fluorescing boutons in the epileptic slices. (**B**) Representative time course of normalized fluorescence intensity of individual boutons from a control (black traces) and a post-status epilepticus (red traces) slice in response to the 600 pulse/20 Hz mossy fibre stimulation (black bar shows duration of the train). (**C**) Normalized, evoked SpH fluorescence increases in response to a 600 pulse/20 Hz mossy fibre stimulus train, in MFBs from control (filled black circles, $F_{peak} = 1.47 \pm 0.03$, $n = 10$) versus post-status epilepticus (open red circles, $F_{peak} = 2.02 \pm 0.15$, $n = 8$) slices. F_{peak} was significantly increased in post-status epilepticus slices ($P < 0.05$, Student's *t*-test; all values mean ± SEM). (**D**) Frequency distribution histogram of normalized peak SpH fluorescence for all MFBs in post-status epilepticus ($F_{peak} = 1.76 \pm 0.04$, 100/115 puncta and 3.89 ± 0.10, 15/115 puncta) versus control slices ($F_{peak} = 1.41 \pm 0.025$, 93 puncta). Inset is a cumulative histogram of normalized peak SpH fluorescence, $P < 0.001$, Kolmogorov–Smirnov test. (**E**) Mean fluorescence values of scaled SpH fluorescence decay (data normalized to respective peak fluorescence values from (**C**) after cessation of stimulation, control (filled black circles) and post-status epilepticus (open red circles). Inset represents mean ± SEM of individual decay constants derived by a single exponential fit to the SpH fluorescence decay curve. Control (black bar), $\tau = 10.4 \pm 0.77$ s, $n = 67$ and post-status epilepticus (red bar), $\tau = 7.23 \pm 0.32$ s, $n = 133$ (*$P < 0.05$, Student's *t*-test). Scale bar: **A** = 5 μm.

To measure presynaptic spontaneous release from the RRP, we loaded FM1-43 by hypertonic shock (800 mOsm/20 s), followed by bath application of tetrodotoxin (1 μM), and extracellular [K^+] raised to 15 mM [K^+]o (*High[K+]o*) to facilitate action potential-independent release (Axmacher *et al.*, 2004). To mark the early phase of action potential-independent release, we monitored the magnitude of FM1-43 destaining within the first 4.5 min of *High[K+]o* application (Fig. 5D), which showed no significant difference between control (~15%) and post-status epilepticus (~20%) MFBs ($P > 0.20$, Student's *t*-test). To determine whether steady-state spontaneous release was altered, we examined the late phase of spontaneous release 10–25 min after application of *High[K+]o* (Fig. 5E). As in the early phase, there was no significant difference between the two groups after 25 min of *High[K+]o*, indicating action potential dependent and independent vesicular release from the RRP are differentially regulated in the post-status epilepticus state.

Status epilepticus elicits long-term ultrastructural reorganization of active zones in rat mossy fibre boutons

Previous literature has shown clear correlations between release probability and synapse morphological parameters such as sizes of the RRP (Dobrunz and Stevens, 1997) and rapidly-recycling

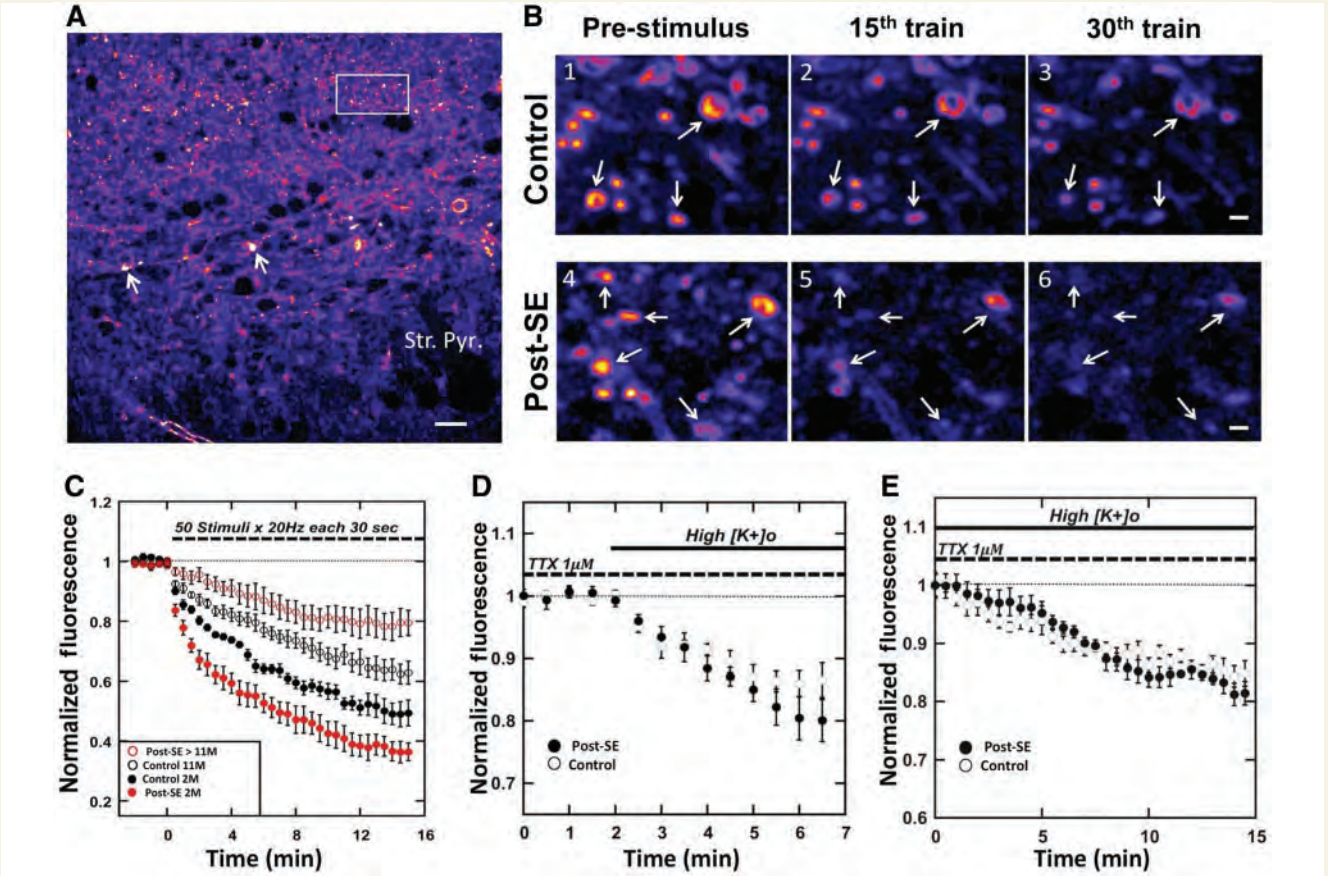

Figure 5 Pilocarpine-induced status epilepticus (SE) enhances evoked, but not action potential independent, presynaptic vesicular release of FM1-43 from the RRP in MFBs. (**A**) Two-photon image of a control field CA3 showing FM1-43 loaded RRP of MFBs. The solid arrows show staining of giant mossy fibre terminals in the proximal region of CA3 stratum lucidum. The rectangular box outlines FM1-43 staining of puncta distal to the CA3 pyramidal cell bodies and much smaller in size, likely to be associational-commissural synapses. (**B**) Representative time-lapse images of FM1-43 destaining from the RRP using repetitive mossy fibre stimulus bursts (50 stimuli/20 Hz each 30 s) to evoke release from MFBs in control and 2-month post-SE slices, respectively. [**B** (1 and 4)] Pre-stimulus baseline fluorescence, [(**B** (2 and 5)] fluorescence intensity after 15 trains, and [**B** (3 and 6)] fluorescence intensity after 30 trains of mossy fibre stimulation. Solid arrows indicate regions of interest $>2\,\mu m$ in diameter that showed robust stimulus dependent FM1-43 destaining. (**C**) Time course of FM1-43 destaining of MFBs in 1–2 months (2 M) post-SE slices (filled red circles, 0.36 ± 0.03, $n = 6$), aged-matched controls (filled black circles, 0.49 ± 0.04, $n = 5$), >11 month (11 M) post-SE slices (open red circles, 0.79 ± 0.04, $n = 5$) and aged-matched controls (open black circles, 0.62 ± 0.04, $n = 6$). All points are mean ± SEM of normalized fluorescence decay at 30th stimulus burst. $P < 0.05$, Student's *t*-test. (**D**) Time course of first 4.5 min of action potential independent FM1-43 destaining in presence of tetrodotoxin (TTX; 1 μm) and 15 mM [K+]o from the RRP in MFBs of 1–2 months post-SE slices (filled circles, $n = 4$) and aged matched control (open circles, $n = 5$) slices (all points are mean ± SEM). Decay after 4.5 min in *High[K+]o*: Control = 0.86 ± 0.028 (~14% of pre-stimulus baseline) and post-SE = 0.80 ± 0.034 (~20% of pre-stimulus baseline; $P > 0.20$, Student's *t*-test). (**E**) Late phase of spontaneous release. Time course of renormalized spontaneous FM1-43 destaining after 10–25 min in *High[K+]o*. Control normalized destaining = 0.85 ± 0.02 and post-SE destaining = 0.81 ± 0.02 ($P > 0.20$, Student's *t*-test, all points are mean ± SEM). Scale bars: **A** = 20 μm; **B** = 10 μm.

pools (Murthy *et al.*, 1997), active zone size (Schikorski and Stevens, 1997; Matz *et al.*, 2010) also known as 'release sites', postsynaptic density (Schikorski and Stevens, 1997) and presynaptic bouton size (Matz *et al.*, 2010). Since we found increased release probability post-status epilepticus as measured by both SpH (Fig. 4C) and FM1-43 destaining (Fig. 5C), we examined possible ultrastructural rearrangements in MFBs in CA3 stratum lucidum in post-status epilepticus and age-matched control Sprague–Dawley rats (Fig. 6A).

Transmission electron microscopy shows that large MFBs (2–5 μm in diameter) had multiple active zones facing postsynaptic densities, contained mitochondria of various sizes, and were filled with numerous small and large clear synaptic vesicles distributed throughout the terminal (Fig. 6A), as described previously (Amaral and Dent, 1981; Chicurel and Harris, 1992; Rollenhagen *et al.*, 2007). Asymmetric active zones were distinguished at MFBs synapses by the dense accumulation of synaptic vesicles in close proximity to the presynaptic density and characteristic widening of the synaptic cleft.

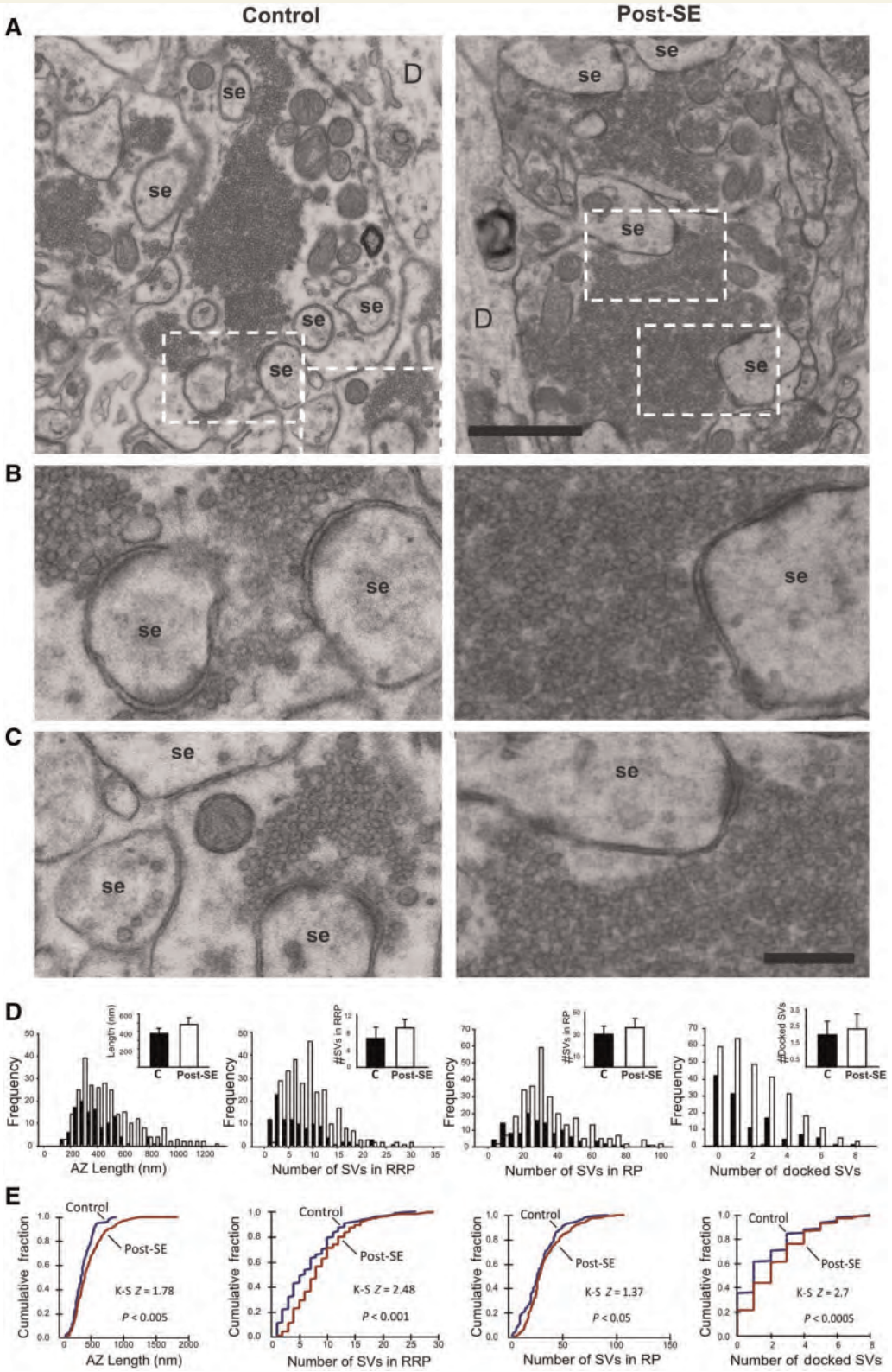

Figure 6 Transmission electron microscopy of active zones (AZ) in MFBs of control and post-status epilepticus (SE) rats. (**A**) Representative transmission electron microscopy images of control (*left*) and post-SE (*right*) MFBs illustrating active zones on synaptic excrescences (se) showing an apparent increase in synaptic vesicle density in post-SE MFBs. Boxed areas are depicted at higher magnification ($\times 4$) in images (**B** and **C**), showing arrangement of vesicles in the active zones of control and post-SE MFBs. Notice the larger density of vesicles and length of active zones in post-SE MFBs. (**D**) Frequency histograms and bar graph representation of data for active zone length, number of synaptic vesicles (SV) in RRP and releasable vesicle pool (RP), and number of docked synaptic vesicles. Notice appearance of increased number of active zones exhibiting larger lengths post-SE (>800 nm). (**E**) Cumulative histograms for these variables in control versus post-SE groups revealed significant rightward shifts toward larger sizes (Kolmogorov–Smirnov (K–S) two-sample test). Scale bars: **A** = 2 μm; **B–E** = 500 nm. D = dendrite.

Table 1 Summary of quantitative analysis of structural variables in active zones of MFBs

	Control, Mean ± SD	Post-status epilepticus, Mean ± SD	Percentage of control	K–S, *P*
Active zone ultrastructural variables				
Length of active zone (nm)	364.91 ± 44.81	485.27 ± 59.63	133.5	*<0.005*
Length of synaptic cleft (nm)	26.93 ± 3.91	29.95 ± 2.46	107.4	*0.31*
PSD area (mm^2)	12.31 ± 3.03	16.90 ± 3.31	136.9	*<0.005*
Number of SVs in RRP	7.43 ± 3.12	8.94 ± 1.78	120.3	*<0.001*
Number of SVs in the releasable pool	31.07 ± 6.05	33.44 ± 7.13	107.6	*<0.05*
Number of docked SVs per active zone	1.96 ± 0.68	2.63 ± 0.56	134.2	*<0.0005*
Docked SVs per active zone length (SV/mm)	5.48 ± 1.75	5.88 ± 0.90	108.9	*<0.05*
Percentage of docked SVs of RRP	27.92 ± 6.45	29.56 ± 3.24	105.85	*0.59*

Measurements were obtained from analysis of active zone variables in MFBs. Statistical comparisons were made using the Kolmogorov–Smirnov (K–S) two-sample test, with statistical significance set at $P < 0.05$. Values are presented as means ± SEM.
PSD = postsynaptic density; SV = synaptic vesicle.

There was a significant increase in number of active zones per MFB in post-status epilepticus rats (130 active zones in six control rats, 5.1 ± 1.36 active zones per MFB; 286 active zones in seven post-status epilepticus rats, 7.7 ± 3.05 active zones per MFB, Student's *t*-test, $P < 0.05$). The number of perforated synapses was also significantly increased in MFBs from post-status epilepticus animals (46 of 286, 16.1%) compared to controls (12 of 130, 9.2%, Student's *t*-test, $P < 0.05$). The majority of electron microscopy variables failed to follow normal distributions, necessitating use of a non-parametric Kolmogorov–Smirnov two-sample test to assess between group differences in distributions. As reported previously (Chicurel and Harris, 1992; Rollenhagen *et al.*, 2007), individual active zones varied substantially in shape and size; both large and small active zones were found in control (104–887 nm) and post-status epilepticus (105–1837 nm) hippocampus. Frequency distributions revealed the presence of a distinct group of synapses of larger length in epileptic animals that was absent in controls (Fig. 6D). A cumulative histogram indicated a significant leftward shift towards larger individual active zone lengths in MFBs post-status epilepticus (Fig. 6E), compared with controls (Table 1, Kolmogorov–Smirnov test, $P < 0.005$). There was also a significant increase in mean postsynaptic density area in the post-status epilepticus group (Table 1) compared to controls (Table 1, Kolmogorov–Smirnov test $P < 0.005$, ~37% increase). In contrast, no significant changes were detected in average synaptic cleft width between control and post-status epilepticus active zones (Table 1).

It has been previously suggested that a rapid refilling of the RRP from a larger releasable vesicle pool is a key mechanism in ensuring fidelity of mossy fibre-CA3 pyramidal cell neurotransmission (Suyama *et al.*, 2007). To determine whether ultrastructural organization of synaptic vesicle pools is altered post-status epilepticus, we measured the number of vesicles docked, within 60 nm of the active zone, 60–200 nm from an active zone, and >200 nm from an active zone, in MFBs of control versus epileptic animals. The RRP was defined as the sum of docked vesicles and those within 60 nm of the active zone, while the releasable pool was defined as vesicles 60–200 nm away from an active zone (Suyama *et al.*, 2007). Compared with controls, post-status epilepticus increased number of docked (+34.2%), RRP (+20.3%), and releasable pool (+7.6%) synaptic vesicles (Fig. 6D and Table 1). A significant difference was detected in the analysis of the cumulative distributions of these variables by Kolmogorov–Smirnov test (Fig. 6E and Table 1). Although the percentage of docked vesicles relative to RRP size was not significantly different (Table 1), the average number of docked vesicles per length of active zone was significantly higher for post-status epilepticus (+8.9%, Table 1). Additionally, the number of synaptic vesicles in each of these pools was significantly correlated with the length of individual active zones in both control (RRP: $r = 0.33$, $P < 0.001$ and releasable pool: $r = 0.41$, $P < 0.001$) and post-status epilepticus MFBs (RRP: $r = 0.57$, $P < 0.001$ and releasable pool: $r = 0.55$, $P < 0.001$, Supplementary Fig. 3).

In order to assess endocytosis, we measured the number and percent of clathrin-coated vesicles 0–200 nm from an active zone (Fig. 7A) and the area of membranous regions apparently internalized at the active zone, indicative of 'bulk endocytosis' (Fig. 7B), in MFBs of control and post-status epilepticus. There were no statistical differences in percent of synapses exhibiting one or two putative clathrin-coated vesicles at active zones between control (22.7 ± 10.1%) and post-status epilepticus (22.0 ± 7.1%, Fig. 7C) animals, or percent synapses exhibiting bulk endocytosis (control: 48.7 ± 13.1%, epileptic: 40.7 ± 15.8%). In contrast, the area of large elliptical or irregular membranous structures at the active zone was significantly higher at MFB synapses post-status epilepticus (5662 ± 385 nm^2) compared with controls (2917 ± 287 nm^2, Kolmogorov–Smirnov test, $P < 0.001$, Fig. 7D), suggesting increased rate of endocytosis.

Taken together, our electron microscopy data show pilocarpine-induced status epilepticus leads to a profound and long-lasting rearrangement of MFB transmitter release sites, resulting in significant increases in number of release sites per MFB, length of individual release sites, and RRP and releasable pool vesicle pools sizes that may underlie persistent increases in functional transmitter vesicular release rates, magnitude and recycling properties.

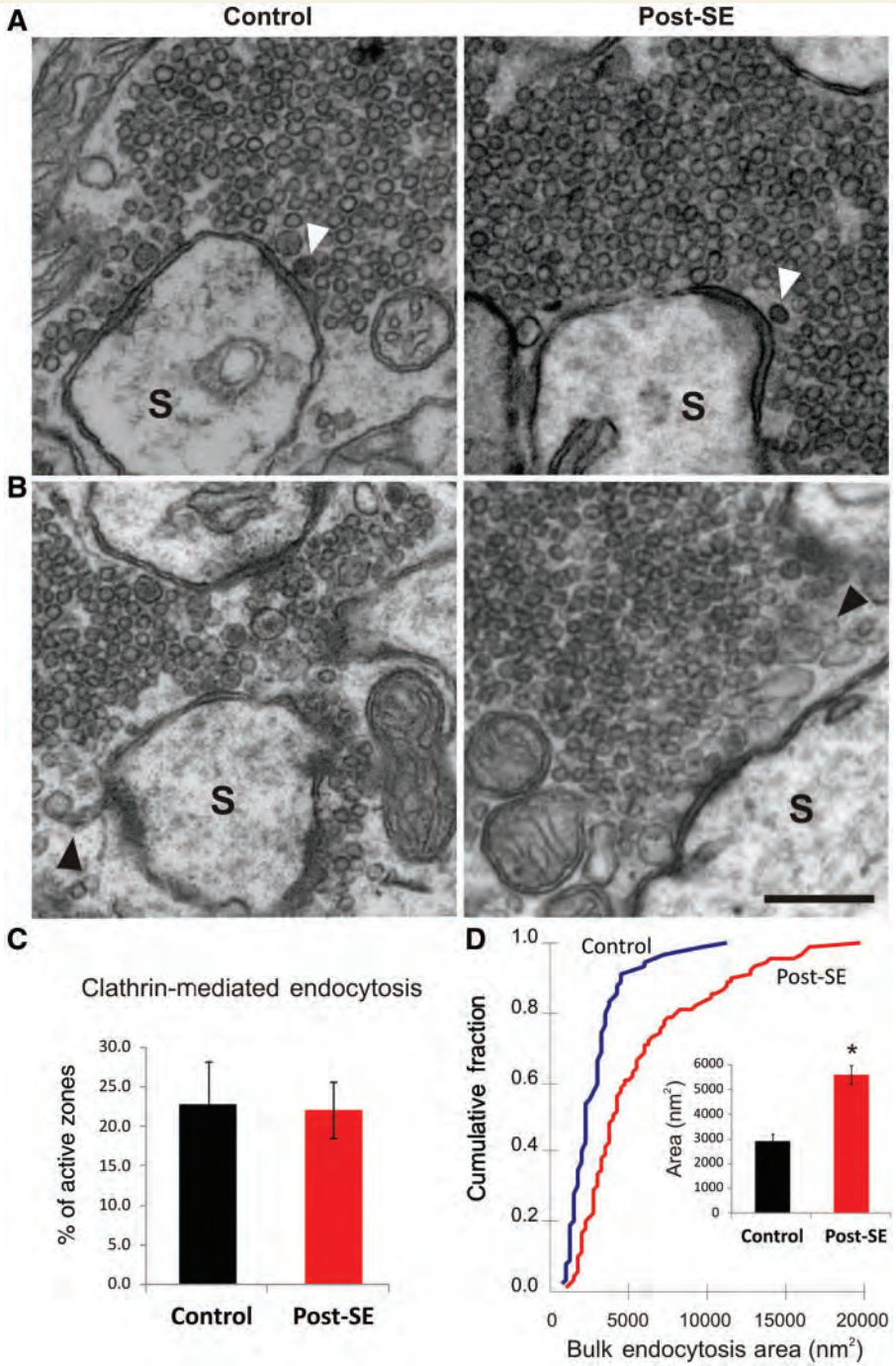

Figure 7 Representative transmission electron microscopy images of active zones in MFBs exhibiting structural signs of clathrin-mediated endocytosis and 'bulk endocytosis' in control versus epileptic rats. (**A**) Putative clathrin-coated (dark) vesicles (white arrowheads) located proximal to presynaptic membrane active zones synapsing on spines (S) of control and post-status epilepticus (SE) MFBs. (**B**) Irregular membranous structures (black arrowheads) near active zones on spines were observed in both control and post-SE MFBs. Note these structures were larger in post-SE rats. (**C**) Mean ± SEM% active zones positive for clathrin-coated vesicles, showing no difference in control versus post-SE rats ($P > 0.20$, Student's *t*-test). (**D**) Cumulative histogram plot of bulk endocytosis area showing a significant rightward shift on the size distribution towards larger values in post-SE MFBs (red) compared with controls (blue, $P < 0.001$, Kolmogorov–Smirnov test). Inset: mean area of bulk endocytosis in control (black) versus post-status epilepticus (red) rats (*$P < 0.05$, Student's *t*-test. Scale bars: **A**, **B** = 500 nm.

Discussion

We describe here a set of long-term alterations in presynaptic morphology and synaptic vesicle recycling at mossy fibre-CA3 terminals of rats and mice subjected to pilocarpine-induced status epilepticus, a model of temporal lobe epilepsy that results in spontaneous recurrent seizures within 2 months in ~97% of rats (Leite *et al.*, 1990; Cavalheiro *et al.*, 1991; Mello *et al.*, 1993; Priel *et al.*, 1996) and mice (Cavalheiro *et al.*, 1996; Muller *et al.*, 2009). In rats, the latent period ranges between 1 and 6 weeks (Curia *et al.*, 2008), with the mean latent period between 15–18 days (Leite *et al.*, 1990; Priel *et al.*, 1996), and depends on the duration of status epilepticus, where a 2-h status epilepticus corresponds to about a 7-day long latent period (Goffin *et al.*, 2007). In mice, the latent period is ~14 days (Cavalheiro *et al.*, 1996), therefore, an overwhelming majority of our animals likely developed spontaneous seizures prior to experiments. Observed presynaptic changes include increases in (i) MFB size; (ii) number of release sites per MFB; (iii) number of vesicles in the RRP and releasable pool; (iv) active zone length; (v) action potential-driven vesicular release rate measured with either FM1-43 or in SpH-expressing transgenic mice; and (vi) enhanced vesicle endocytosis. These alterations persisted for at least 1 month following a single sustained status epilepticus.

Functional enhancement in vesicular transmitter release from MFBs correlates well with previously reported structural changes (number of docked synaptic vesicles or the RRP, area of postsynaptic density, active zone length) that track vesicle release probability (Schikorski and Stevens, 1997; Matz *et al.*, 2010), suggesting that the morphological changes are probably components of the response to hyperactivation that underlie enhanced transmitter release. This agrees with a previous report that kainic acid-induced seizures lead to an increase in glutamate release from the RRP and loss of paired pulse facilitation (Goussakov *et al.*, 2000), suggesting that seizures of a variety of causes may lead to persistent increases in basal release probability.

The significant increase we observed in FM1-43 destaining post-status epilepticus and the correlated increase of vesicle pool sizes measured by transmission electron microscopy suggest an increase in both initial release probability and size of the readily releasable and rapidly recycling vesicle pools. Previous reports suggest that the size of the recycling pool is an important determinant of sustainability of release with prolonged activation (Suyama *et al.*, 2007), consistent with the increases we observed post-status epilepticus. While our transmission electron microscopy SpH and Alexa Fluor 594-dextran loading data all indicate that MFBs show increased size and larger numbers of synaptic vesicles for months after status epilepticus; the new population of terminals, with significantly larger size and faster release rate, could be from modification of existing terminals, ectopic MFBs, or both, and remains to be determined. Also, since individual MFBs contain multiple active zones (Hallermann *et al.*, 2003), we cannot tell whether increased release probability at MFBs (Figs 4D and 5C) occurs at the level of individual active zones switching to a high release state, or whether there is a uniform increase in release probability across all active zones. Additional changes such as increases in the number of active zones per bouton and size of the RRP and releasable pool in individual active zones also suggest persistent increase in glutamate release that could be a key contributor to death of CA3 pyramidal neurons characteristic of hippocampal sclerosis. Increases in the density of perforated synapses have been associated with synaptogenesis and post-lesional compensatory plasticity (Itarat and Jones, 1992; Luke *et al.*, 2004; Adkins *et al.*, 2008). Increased incidence of perforated mossy fibre synapses after status epilepticus suggest that synaptic connectivity undergoes structural remodelling favouring synapses, with potentially higher transmission efficiency during the process of epileptogenesis.

Using SpH fluorescence, we derived a decay constant of 10.4 ± 0.77 s for control boutons (Fig. 4E), similar to previous reports of an endocytic time constant of 9.0 ± 5.5 s estimated using capacitance recordings at MFBs (Hallermann *et al.*, 2003). Our observations of accelerated recovery of stimulus-evoked SpH fluorescence in slices from post-status epilepticus mice, but lack of differences between the number of clathrin-coated vesicles in electromicrographs between the post-status epilepticus and control groups, could be due to an enhanced rate of endocytosis that may or may not depend on clathrin, increased local recycling of vesicles to the RRP (Stanton *et al.*, 2003) or to the recycling pool after exocytosis (Wu and Wu, 2009), increase in bulk endocytosis (retrieval of larger membrane area, Table 1) or combinations of the above. Also, tissues used for electromicrographs were not electrically stimulated prior to fixation, and thus do not necessarily reflect activity-dependent endocytic events but, more likely, the steady-state of the presynaptic bouton ultrastructure.

The 1–2 month time point post-status epilepticus used in our experiments corresponds to the period of occurrence of spontaneous seizures in both rats (Leite *et al.*, 1990; Cavalheiro *et al.*, 1991; Priel *et al.*, 1996; Dudek and Sutula, 2007) and mice (Cavalheiro *et al.*, 1996; Muller *et al.*, 2009; Schauwecker, 2012). Interestingly, in contrast to the early increase in MFB release probability, we found that, at very long survival periods post-status epilepticus (11–12 months), rates of MFB release were markedly reduced. The reduced transmitter release from the RRP in these animals could either reflect long-term compensatory changes or dysfunction of presynaptic release machinery. Our observation that action potential independent RRP release rate in tetrodotoxin (1 μm) was not altered by pilocarpine seizures indicates that action potential dependent and independent regulation of the RRP is very different, perhaps due to potentially distinct pools of vesicles and mechanisms between evoked and spontaneous release (Fredj and Burrone, 2009; Chung *et al.*, 2010). We cannot rule out the possibility that new vesicle pools may contribute to action potential independent release of glutamate post-status epilepticus.

Our functional data demonstrating that post-status epilepticus state leads to increased vesicular release and endocytotic rates, and electron microscope data showing increased presynaptic active zone length, membrane invaginations, clathrin-coated vesicles and vesicle pool sizes, are all consistent with the conclusion that post-status epilepticus state is associated with long-term increases in transmitter release from MFBs, and perhaps other glutamatergic terminals. Since brain-derived neurotrophic factor

is highly expressed in presynaptic MFBs (Danzer and McNamara, 2004) and can elicit long-term enhancements in both transmitter release and size of the RRP (Zakharenko *et al.*, 2003; Tyler *et al.*, 2006), neurotrophins seem a likely candidate mediator of these presynaptic alterations.

Whether increase in stimulus evoked release following-status epilepticus results from alterations in Ca^{2+} influx, release of Ca^{2+} from internal stores *per se*, or whether there are downstream changes in SNARE protein sensitivity to Ca^{2+} is not known. A recent study (Pacheco *et al.*, 2008) found that pilocarpine seizures also cause downregulation of large conductance calcium-activated potassium (BK) channels in MFBs, reductions that could slow hyperpolarization and increase terminal Ca^{2+} influx. Levels of the Ca^{2+} buffer calbindin D-28K are also lowered in MFBs after pilocarpine seizures (Carter *et al.*, 2008), a change that could further increase presynaptic Ca^{2+} influx, dysregulate Ca^{2+} homeostasis and promote multivesicular release (Hallermann *et al.*, 2003).

In summary, our study is the first, to our knowledge, using the pilocarpine model of temporal lobe epilepsy in SpH-expressing transgenic mice, a new tool to investigate presynaptic alterations in epilepsy with potential application for other CNS diseases that may involve presynaptic dysfunction. Our studies indicate that the early phase of the pilocarpine model of temporal lobe epilepsy is associated with persistent structural changes in mossy fibre presynaptic terminal size, vesicle pools and active zones that are correlated with functional increases in rates of action potential-driven vesicular release and associated endocytotic recycling. The time course and mechanisms underlying these changes suggests the presynaptic terminal as a novel target for new therapeutics to treat epilepsy, especially temporal lope epilepsy.

Acknowledgements

The authors would like to thank Dr Venkatesh Murthy for providing us with the SpH21 transgenic mice line, Dr Kenichi Miyazaki for help with Alexa Fluor 594 dextran experiments, Mohini Rawat for technical assistance, Dr Pravin Sehgal and Jason Lee for discussions on Otsu thresholding and Dr Xiao-Lei Zhang and John Sullivan for additional helpful discussions.

Funding

National Institutes of Health (grants GM081109, P20 MD001091-06 and NS063950); Department of Defense (grant PR100534 to E.R.G.S.); National Institute of Neurological Diseases and Stroke (grants NS056093 to J.V., NS072966 to L.V. and NS044421 to P.K.S.); Department of Defense (grant PR100534P1 to P.K.S.).

Supplementary material

Supplementary material is available at *Brain* online.

References

Acsady L, Kamondi A, Sik A, Freund T, Buzsaki G. GABAergic cells are the major postsynaptic targets of mossy fibers in the rat hippocampus. J Neurosci 1998; 18: 3386–403.

Adkins DL, Hsu JE, Jones TA. Motor cortical stimulation promotes synaptic plasticity and behavioral improvements following sensorimotor cortex lesions. Exp Neurol 2008; 212: 14–28.

Amaral DG, Dent JA. Development of the mossy fibers of the dentate gyrus: I. A light and electron microscopic study of the mossy fibers and their expansions. J Comp Neurol 1981; 195: 51–86.

Axmacher N, Winterer J, Stanton PK, Draguhn A, Muller W. Two-photon imaging of spontaneous vesicular release in acute brain slices and its modulation by presynaptic GABAA receptors. Neuroimage 2004; 22: 1014–21.

Bailey CP, Nicholls RE, Zhang XL, Zhou ZY, Muller W, Kandel ER, et al. Galpha(i2) inhibition of adenylate cyclase regulates presynaptic activity and unmasks cGMP-dependent long-term depression at Schaffer collateral-CA1 hippocampal synapses. Learn Mem 2008; 15: 261–70.

Bayazitov IT, Richardson RJ, Fricke RG, Zakharenko SS. Slow presynaptic and fast postsynaptic components of compound long-term potentiation. J Neurosci 2007; 27: 11510–21.

Bischofberger J, Engel D, Li L, Geiger JR, Jonas P. Patch-clamp recording from mossy fiber terminals in hippocampal slices. Nat Protoc 2006; 1: 2075–81.

Blackstad TW, Brink K, Hem J, Jeune B. Distribution of hippocampal mossy fibers in the rat. An experimental study with silver impregnation methods. J Comp Neurol 1970; 138: 433–49.

Boulland JL, Ferhat L, Tallak Solbu T, Ferrand N, Chaudhry FA, Storm-Mathisen J, et al. Changes in vesicular transporters for gamma-aminobutyric acid and glutamate reveal vulnerability and reorganization of hippocampal neurons following pilocarpine-induced seizures. J Comp Neurol 2007; 503: 466–85.

Burrone J, Li Z, Murthy VN. Studying vesicle cycling in presynaptic terminals using the genetically encoded probe synaptopHluorin. Nat Protoc 2006; 1: 2970–8.

Calverley RK, Jones DG. Determination of the numerical density of perforated synapses in rat neocortex. Cell Tissue Res 1987; 248: 399–407.

Carter DS, Harrison AJ, Falenski KW, Blair RE, DeLorenzo RJ. Long-term decrease in calbindin-D28K expression in the hippocampus of epileptic rats following pilocarpine-induced status epilepticus. Epilepsy Res 2008; 79: 213–23.

Cavalheiro EA. The pilocarpine model of epilepsy. Ital J Neurol Sci 1995; 16: 33–7.

Cavalheiro EA, Leite JP, Bortolotto ZA, Turski WA, Ikonomidou C, Turski L. Long-term effects of pilocarpine in rats: structural damage of the brain triggers kindling and spontaneous recurrent seizures. Epilepsia 1991; 32: 778–82.

Cavalheiro EA, Santos NF, Priel MR. The pilocarpine model of epilepsy in mice. Epilepsia 1996; 37: 1015–9.

Cavazos JE, Zhang P, Qazi R, Sutula TP. Ultrastructural features of sprouted mossy fiber synapses in kindled and kainic acid-treated rats. J Comp Neurol 2003; 458: 272–92.

Chicurel ME, Harris KM. Three-dimensional analysis of the structure and composition of CA3 branched dendritic spines and their synaptic relationships with mossy fiber boutons in the rat hippocampus. J Comp Neurol 1992; 325: 169–82.

Chung C, Barylko B, Leitz J, Liu X, Kavalali ET. Acute dynamin inhibition dissects synaptic vesicle recycling pathways that drive spontaneous and evoked neurotransmission. J Neurosci 2010; 30: 1363–76.

Claiborne BJ, Amaral DG, Cowan WM. A light and electron microscopic analysis of the mossy fibers of the rat dentate gyrus. J Comp Neurol 1986; 246: 435–58.

Coulter DA. Mossy fiber zinc and temporal lobe epilepsy: pathological association with altered "epileptic" gamma-aminobutyric acid A receptors in dentate granule cells. Epilepsia 2000; 41 (Suppl 6): S96–9.

Curia G, Longo D, Biagini G, Jones RS, Avoli M. The pilocarpine model of temporal lobe epilepsy. J Neurosci Methods 2008; 172: 143–57.

Danzer SC, He X, Loepke AW, McNamara JO. Structural plasticity of dentate granule cell mossy fibers during the development of limbic epilepsy. Hippocampus 2010; 20: 113–24.

Danzer SC, McNamara JO. Localization of brain-derived neurotrophic factor to distinct terminals of mossy fiber axons implies regulation of both excitation and feedforward inhibition of CA3 pyramidal cells. J Neurosci 2004; 24: 11346–55.

Dobrunz LE, Stevens CF. Heterogeneity of release probability, facilitation, and depletion at central synapses. Neuron 1997; 18: 995–1008.

Dudek FE, Sutula TP. Epileptogenesis in the dentate gyrus: a critical perspective. Prog Brain Res 2007; 163: 755–73.

Epsztein J, Represa A, Jorquera I, Ben-Ari Y, Crepel V. Recurrent mossy fibers establish aberrant kainate receptor-operated synapses on granule cells from epileptic rats. J Neurosci 2005; 25: 8229–39.

Esclapez M, Hirsch JC, Ben-Ari Y, Bernard C. Newly formed excitatory pathways provide a substrate for hyperexcitability in experimental temporal lobe epilepsy. J Comp Neurol 1999; 408: 449–60.

Fredj NB, Burrone J. A resting pool of vesicles is responsible for spontaneous vesicle fusion at the synapse. Nat Neurosci 2009; 12: 751–8.

Frotscher M, Jonas P, Sloviter RS. Synapses formed by normal and abnormal hippocampal mossy fibers. Cell Tissue Res 2006; 326: 361–7.

Galimberti I, Gogolla N, Alberi S, Santos AF, Muller D, Caroni P. Long-term rearrangements of hippocampal mossy fiber terminal connectivity in the adult regulated by experience. Neuron 2006; 50: 749–63.

Goffin K, Nissinen J, Van Laere K, Pitkanen A. Cyclicity of spontaneous recurrent seizures in pilocarpine model of temporal lobe epilepsy in rat. Exp Neurol 2007; 205: 501–5.

Gorter JA, Goncalves Pereira PM, van Vliet EA, Aronica E, Lopes da Silva FH, Lucassen PJ. Neuronal cell death in a rat model for mesial temporal lobe epilepsy is induced by the initial status epilepticus and not by later repeated spontaneous seizures. Epilepsia 2003; 44: 647–58.

Gorter JA, Van Vliet EA, Proper EA, De Graan PN, Ghijsen WE, Lopes Da Silva FH, et al. Glutamate transporter alterations in the reorganizing dentate gyrus are associated with progressive seizure activity in chronic epileptic rats. J Comp Neurol 2002; 442: 365–77.

Goussakov IV, Fink K, Elger CE, Beck H. Metaplasticity of mossy fiber synaptic transmission involves altered release probability. J Neurosci 2000; 20: 3434–41.

Hallermann S, Pawlu C, Jonas P, Heckmann M. A large pool of releasable vesicles in a cortical glutamatergic synapse. Proc Natl Acad Sci USA 2003; 100: 8975–80.

Hovorka J, Langmeier M, Mares P. Are there morphological changes in presynaptic terminals of kindled rats? Neurosci Lett 1989; 107: 179–83.

Itarat W, Jones DG. Perforated synapses are present during synaptogenesis in rat neocortex. Synapse 1992; 11: 279–86.

Lee JE, Patel K, Almodovar S, Tuder RM, Flores SC, Sehgal PB. Dependence of Golgi apparatus integrity on nitric oxide in vascular cells: implications in pulmonary arterial hypertension. Am J Physiol Heart Circ Physiol 2011; 300: H1141–58.

Leite JP, Bortolotto ZA, Cavalheiro EA. Spontaneous recurrent seizures in rats: an experimental model of partial epilepsy. Neurosci Biobehav Rev 1990; 14: 511–7.

Li Z, Burrone J, Tyler WJ, Hartman KN, Albeanu DF, Murthy VN. Synaptic vesicle recycling studied in transgenic mice expressing synaptopHluorin. Proc Natl Acad Sci USA 2005; 102: 6131–6.

Luke LM, Allred RP, Jones TA. Unilateral ischemic sensorimotor cortical damage induces contralesional synaptogenesis and enhances skilled reaching with the ipsilateral forelimb in adult male rats. Synapse 2004; 54: 187–99.

Matz J, Gilyan A, Kolar A, McCarvill T, Krueger SR. Rapid structural alterations of the active zone lead to sustained changes in neurotransmitter release. Proc Natl Acad Sci USA 2010; 107: 8836–41.

McNamara JO. Cellular and molecular basis of epilepsy. J Neurosci 1994; 14: 3413–25.

Mello LE, Cavalheiro EA, Tan AM, Kupfer WR, Pretorius JK, Babb TL, et al. Circuit mechanisms of seizures in the pilocarpine model of chronic epilepsy: cell loss and mossy fiber sprouting. Epilepsia 1993; 34: 985–95.

Meunier FA, Nguyen TH, Colasante C, Luo F, Sullivan RK, Lavidis NA, et al. Sustained synaptic-vesicle recycling by bulk endocytosis contributes to the maintenance of high-rate neurotransmitter release stimulated by glycerotoxin. J Cell Sci 2010; 123 (Pt 7): 1131–40.

Miesenbock G, De Angelis DA, Rothman JE. Visualizing secretion and synaptic transmission with pH-sensitive green fluorescent proteins. Nature 1998; 394: 192–5.

Miranda R, Nudel U, Laroche S, Vaillend C. Altered presynaptic ultrastructure in excitatory hippocampal synapses of mice lacking dystrophins Dp427 or Dp71. Neurobiol Dis 2011; 43: 134–41.

Muller CJ, Bankstahl M, Groticke I, Loscher W. Pilocarpine vs. lithium-pilocarpine for induction of status epilepticus in mice: development of spontaneous seizures, behavioral alterations and neuronal damage. Eur J Pharmacol 2009; 619: 15–24.

Murthy VN, Sejnowski TJ, Stevens CF. Heterogeneous release properties of visualized individual hippocampal synapses. Neuron 1997; 18: 599–612.

Pacheco Otalora LF, Couoh J, Shigamoto R, Zarei MM, Garrido Sanabria ER. Abnormal mGluR2/3 expression in the perforant path termination zones and mossy fibers of chronically epileptic rats. Brain Res 2006; 1098: 170–85.

Pacheco Otalora LF, Hernandez EF, Arshadmansab MF, Francisco S, Willis M, Ermolinsky B, et al. Down-regulation of BK channel expression in the pilocarpine model of temporal lobe epilepsy. Brain Res 2008; 1200: 116–31.

Priel MR, dos Santos NF, Cavalheiro EA. Developmental aspects of the pilocarpine model of epilepsy. Epilepsy Res 1996; 26: 115–21.

Pyle JL, Kavalali ET, Choi S, Tsien RW. Visualization of synaptic activity in hippocampal slices with FM1-43 enabled by fluorescence quenching. Neuron 1999; 24: 803–8.

Rollenhagen A, Satzler K, Rodriguez EP, Jonas P, Frotscher M, Lubke JH. Structural determinants of transmission at large hippocampal mossy fiber synapses. J Neurosci 2007; 27: 10434–44.

Sankaranarayanan S, Ryan TA. Real-time measurements of vesicle-SNARE recycling in synapses of the central nervous system. Nat Cell Biol 2000; 2: 197–204.

Schauwecker PE. Strain differences in seizure-induced cell death following pilocarpine-induced status epilepticus. Neurobiol Dis 2012; 45: 297–304.

Schikorski T, Stevens CF. Quantitative ultrastructural analysis of hippocampal excitatory synapses. J Neurosci 1997; 17: 5858–67.

Stanton PK, Winterer J, Bailey CP, Kyrozis A, Raginov I, Laube G, et al. Long-term depression of presynaptic release from the readily releasable vesicle pool induced by NMDA receptor-dependent retrograde nitric oxide. J Neurosci 2003; 23: 5936–44.

Stanton PK, Winterer J, Zhang XL, Muller W. Imaging LTP of presynaptic release of FM1-43 from the rapidly recycling vesicle pool of Schaffer collateral-CA1 synapses in rat hippocampal slices. Eur J Neurosci 2005; 22: 2451–61.

Suyama S, Hikima T, Sakagami H, Ishizuka T, Yawo H. Synaptic vesicle dynamics in the mossy fiber-CA3 presynaptic terminals of mouse hippocampus. Neurosci Res 2007; 59: 481–90.

Turski WA, Cavalheiro EA, Bortolotto ZA, Mello LM, Schwarz M, Turski L. Seizures produced by pilocarpine in mice: a behavioral, electroencephalographic and morphological analysis. Brain Res 1984; 321: 237–53.

Tyler WJ, Zhang XL, Hartman K, Winterer J, Muller W, Stanton PK, et al. BDNF increases release probability and the size of a rapidly recycling vesicle pool within rat hippocampal excitatory synapses. J Physiol 2006; 574 (Pt 3): 787–803.

Wenzel HJ, Woolley CS, Robbins CA, Schwartzkroin PA. Kainic acid-induced mossy fiber sprouting and synapse formation in the dentate gyrus of rats. Hippocampus 2000; 10: 244–60.

Winterer J, Stanton PK, Muller W. Direct monitoring of vesicular release and uptake in brain slices by multiphoton excitation of the styryl dye FM 1-43. Biotechniques 2006; 40: 343–51.

Wu XS, Wu LG. Rapid endocytosis does not recycle vesicles within the readily releasable pool. J Neurosci 2009; 29: 11038–42.

Xiong ZQ, Stringer JL. Extracellular pH responses in CA1 and the dentate gyrus during electrical stimulation, seizure discharges, and spreading depression. J Neurophysiol 2000; 83: 3519–24.

Zakharenko SS, Patterson SL, Dragatsis I, Zeitlin SO, Siegelbaum SA, Kandel ER, et al. Presynaptic BDNF required for a presynaptic but not postsynaptic component of LTP at hippocampal CA1-CA3 synapses. Neuron 2003; 39: 975–90.

Zhang S, Khanna S, Tang FR. Patterns of hippocampal neuronal loss and axon reorganization of the dentate gyrus in the mouse pilocarpine model of temporal lobe epilepsy. J Neurosci Res 2009; 87: 1135–49.

Control/Tracking Number: 2012-S-11204-SfN
Activity: Scientific Abstract
Current Date/Time: 5/14/2012 3:33:40 PM

Levetiracetam inhibits excitatory drive onto dentate gyrus granule cells: Effects of SV2A gene dosage and mesial temporal lobe epilepsy.

AUTHOR BLOCK: *E. G. SANABRIA[1], L. F. PACHECO[2], L. M. RAMBO[2], J. M. RODRIGUEZ[2], C. UPRETI[3], P. K. STANTON[4];
[1]Biomedicine, Univ. of Texas Brownsville, BROWNSVILLE, TX; [2]Biomedicine, Univ. of Texas at Brownsville, BROWNSVILLE, TX; [3]Dept. of Cell Biol. & Anat., [4]Cell Biol. & Anat. and Dept. of Neurol., New York Med. Col., Valhalla, NY

Abstract:
Levetiracetam (LEV) is a new type of antiepileptic drug (AED) exhibiting selective seizure protection in chronic animal models of epilepsy. LEV binds selectively to the synaptic vesicle protein SV2A, indicating a presynaptic site of action to counter hyperexcitability. In this study, we evaluated the in vitro effects of LEV on excitatory synaptic transmission in the pilocarpine model of mesial temporal lobe epilepsy (MTLE). It has been reported that expression levels of SV2A decline during the course of human epilepsy and in experimental MTLE. We hypothesized that LEV action may be differentially affected during epileptogenesis and in transgenic mice with altered SV2A expression. For this purpose, we assessed LEV effects on excitatory synaptic transmission in slices from pilocarpine-treated epileptic and control mice with different SV2A genotypes, by recording AMPA receptor-mediated miniature excitatory postsynaptic currents (mEPSCs) in dentate granule cells using whole cell patch-clamp recording. Different concentrations of LEV (5, 50 and 100 microM) were bath applied to evaluate effects on mEPSC frequency and amplitude. Double SV2A/SV2B knockout (KO) mice were not included in this study due to early life mortality. 14% of SV2A heterozygous KO mice exhibited spontaneous seizures (epileptic). LEV induced a significant decrease of mEPSC frequency in granule cells from SV2A wild-type (26% reduction) and heterozygous mice (37% reduction) when compared to pre-drug baseline. LEV (100 μM) failed to modify mEPSC frequency in ~ 60% of slices from SV2A KO mice, while a paradoxical increase of mEPSC frequency was detected in the rest of the slices. LEV still induced a significant decrease of mEPSC frequency (51.7% reduction, paired t-test, $P<0.05$) in slices from SV2A/SV2B (wild-type) mice sacrificed 2-4 months after status epilepticus. LEV exerted no significant effects on mEPSC amplitude in any group. Our findings indicate that LEV acts presynaptically to inhibit glutamatergic drive onto dentate granule cells in control and chronically epileptic mice, but that this effect is more pronounced in epileptic slices. Lack of SV2A expression occluded the inhibitory effect of LEV on excitatory transmission in a subset of animals, while a paradoxical increase of glutamate release was detected in the rest. Although LEV selectively binds SV2A in normal brain, it is possible that compensatory changes (i.e. abnormal splicing) of remaining SV2B and SV2C proteins may provide additional non-SV2A LEV binding sites in SV2A KO and in epileptic mice with significant implications for the development of novel LEV-like AEDs.
:

Presentation Preference (Complete): Poster Only

Linking Group (Complete): None selected
Nanosymposium Information (Complete):
Theme and Topic (Complete): C.07.k. Anticonvulsant and antiepileptic therapies ; C.07.e. Synaptic mechanisms
Keyword (Complete): EPILEPSY ; SYNAPTIC TRANSMISSION ; PRESYNAPTIC
Support (Complete):
Support: Yes
Grant/Other Support: : DoD Grant PR100534
Grant/Other Support: : DoD Grant PR100534P1
Grant/Other Support: : NIH Grant NS063950
Grant/Other Support: : NIH Grant GM081109

Special Requests (Complete):
Is the first (presenting) author of this abstract a high school or undergraduate student?: None

Religious Conflict?: No Religious Conflict
Additional Conflict?: No

Status: Finalized